

DNA hypomethylation leads to cGAS-induced autoinflammation in the epidermis

Mirjam A Beck^{1,†}, Heinz Fischer^{1,†}, Lisa M Grabner¹, Tamara Groffics^{1,‡}, Mircea Winter¹, Simone Tangermann², Tina Meischel^{1,§}, Barbara Zaussinger-Haas¹, Patrick Wagner¹, Carina Fischer¹, Christina Folie^{1,3}, Julia Arand¹ , Christian Schöfer¹, Bernard Ramsahoye⁴, Sabine Lagger² , Georg Machat¹, Gregor Eisenwort^{5,¶}, Stephanie Schneider^{1,#}, Alexandra Podhornik¹ , Michael Kothmayer¹, Ursula Reichart⁶, Martin Glösmann⁶, Ido Tamir⁷, Michael Mildner⁸ , Raheleh Sheibani-Tezerji⁹ , Lukas Kenner^{2,10,11,12} , Peter Petzelbauer¹³ , Gerda Egger^{9,11}, Maria Sibilina¹⁴ , Andrea Ablasser¹⁵ & Christian Seiser^{1,*} 

Abstract

DNA methylation is a fundamental epigenetic modification, important across biological processes. The maintenance methyltransferase DNMT1 is essential for lineage differentiation during development, but its functions in tissue homeostasis are incompletely understood. We show that epidermis-specific DNMT1 deletion severely disrupts epidermal structure and homeostasis, initiating a massive innate immune response and infiltration of immune cells. Mechanistically, DNA hypomethylation in keratinocytes triggered transposon derepression, mitotic defects, and formation of micronuclei. DNA release into the cytosol of DNMT1-deficient keratinocytes activated signaling through cGAS and STING, thus triggering inflammation. Our findings show that disruption of a key epigenetic mark directly impacts immune and tissue homeostasis, and potentially impacts our understanding of autoinflammatory diseases and cancer immunotherapy.

Keywords autoinflammation; cytosolic DNA; DNA methylation; epigenetics; innate immune system

Subject Categories Chromatin, Transcription & Genomics; Immunology

DOI 10.15252/embj.2021108234 | Received 13 March 2021 | Revised 28 August 2021 | Accepted 31 August 2021 | Published online 29 September 2021

The EMBO Journal (2021) 40: e108234

Introduction

As the outermost organ of the body, the skin is continuously exposed to pathogens and plays a critical role in the defense against the environment and infectious agents. The most superficial layer of the skin, the epidermis, functions as a critical barrier against viruses, bacteria, and fungi (Alonso & Fuchs, 2003; Fuchs & Horsley, 2008). Various immune cell types reside in the skin or are recruited to maintain skin homeostasis upon exposure to pathogens, including innate immune cells (Kabashima *et al.*, 2019; Nguyen & Soulika,

- 1 Division of Cell and Developmental Biology, Center for Anatomy and Cell Biology, Medical University of Vienna, Vienna, Austria
- 2 Unit of Laboratory Animal Pathology, University of Veterinary Medicine, Vienna, Austria
- 3 Spinal Cord Injury and Tissue Regeneration Center Salzburg (SCI-TReCS), Salzburg, Austria
- 4 MRC Institute of Genetics & Molecular Medicine, Centre for Genomic & Experimental Medicine, University of Edinburgh, Edinburgh, UK
- 5 Institute of Immunology, Medical University of Vienna, Vienna, Austria
- 6 VetCORE - Facility for Research, University of Veterinary Medicine Vienna, Vienna, Austria
- 7 Campus Science Support Facilities GmbH, Vienna, Austria
- 8 Research Division of Biology and Pathobiology of the Skin, Medical University of Vienna, Vienna, Austria
- 9 Ludwig Boltzmann Institute Applied Diagnostics, Vienna, Austria
- 10 Christian Doppler Laboratory for Applied Metabolomics, Vienna, Austria
- 11 Department of Pathology, Medical University of Vienna, Vienna, Austria
- 12 CBmed GmbH - Center for Biomarker Research in Medicine, Graz, Austria
- 13 Skin and Endothelium Research Division, Department of Dermatology, Medical University of Vienna, Vienna, Austria
- 14 Department of Medicine I, Comprehensive Cancer Center, Institute of Cancer Research, Medical University of Vienna, Vienna, Austria
- 15 Global Health Institute, Swiss Federal Institute of Technology Lausanne (EPFL), Lausanne, Switzerland

*Corresponding author. Tel: +43 1 40160 37507; E-mail: christian.seiser@meduniwien.ac.at

[†]These authors contributed equally to this work

[‡]Present address: Max Perutz Labs, Vienna BioCenter, Vienna, Austria

[§]Present address: Department of Microbiology and Immunology, The University of Melbourne at The Peter Doherty Institute for Infection and Immunity, Melbourne, Vic., Australia

[¶]Present address: Department of Hematology and Hemostaseology, Clinic for Internal Medicine I, Medical University of Vienna, Vienna, Austria

[#]Present address: Gene Center - Max von Pettenkofer-Institute of Virology, Ludwig-Maximilians-Universität München, München, Germany

2019). Pathogen-derived nucleic acids are an important signal for innate immunity and detected through specific RNA- and DNA-sensing mechanisms. These mammalian systems distinguish self from non-self through attributes including intracellular localization, secondary structure, post-transcriptional modifications, and abundance of specific nucleic acids (Roers *et al*, 2016; Schlee & Hartmann, 2016; Bartok & Hartmann, 2020). A major mechanism for cytosolic DNA detection is the cGAS/STING pathway (Ablasser & Hur, 2020). The cGAS protein is a central receptor for cytosolic double-stranded DNA that mediates the upregulation of type I interferons and other inflammatory cytokines and chemokines. This occurs via STING activation by the cyclic dinucleotide cGAMP and results in phosphorylation and nuclear translocation of IRF3. The cGAS/STING pathway also plays an important role in the recognition of malignant cells by the immune system (Flood *et al*, 2019; Hoong *et al*, 2020; Kwon & Bakhoun, 2020; Yum *et al*, 2020).

The epidermis is a key context for the operation of the innate immune system and is a self-renewing tissue that requires precise spatiotemporal control of gene expression (Alonso & Fuchs, 2003; Mikkola, 2007). This is achieved through a well-orchestrated interplay between transcription factors and epigenetic regulators mediating the regulation of gene expression (Miroshnikova *et al*, 2019). Heritable CpG methylation is probably the best-studied epigenetic mechanism in mammalian organisms. DNA methylation is mediated by DNA methyltransferases (DNMTs) and plays an important role during development by repressing gamete-specific genes or entire chromosomes such as mammalian X chromosome inactivation (Schubeler, 2015; Ambrosi *et al*, 2017). DNMTs are also involved in the control of allele-specific gene expression and silencing of repetitive elements, thereby maintaining genome integrity (Ambrosi *et al*, 2017). Among the five known members of the DNMT family, DNMT1, DNMT3A, and DNMT3B play an important role during mouse development (Smith & Meissner, 2013). DNMT3A and DNMT3B are known as the *de novo* DNA methyltransferases showing high activity toward unmethylated DNA (reviewed in Espada & Esteller, 2010; Karemaker & Baubec, 2020). DNMT1 has substrate specificity for hemimethylated DNA, but can also transfer the methyl group to unmethylated DNA templates and is therefore considered as the maintenance methyltransferase (reviewed in Mohan and Chaillet (2013) and Karemaker and Baubec (2020)). Of note, DNMTs are relevant targets for small molecule inhibitors in cancer treatment and specific DNMT inhibitors are FDA-approved for the treatment of acute myeloid leukemia (Jones *et al*, 2016).

Several severe chronic inflammatory skin diseases, including psoriasis and atopic dermatitis, show abnormal DNA methylation at genes regulating epidermal differentiation and innate immune response in the epidermis of patients as well as in their T cells (Gudjonsson & Krueger, 2012; Han *et al*, 2012; Rodriguez *et al*, 2014). In these diseases, the defective DNA methylation is accompanied by disruptions in both keratinocyte differentiation and the barrier function of the skin. Several studies suggest that the appearance of various inflammatory skin diseases and autoimmune disorders, as well as skin cancer, stems from altered epigenetic mechanisms (Javierre *et al*, 2012).

A function for DNA methylation in epidermal self-renewal and differentiation was previously described using human *DNMT1* knockdown keratinocytes in immunodeficient mice (Sen *et al*, 2010). This study linked DNMT1 to the maintenance of progenitor

function in the epidermis and its deletion resulted in premature differentiation and tissue loss. In another study, epidermal DNMT1 disruption in aging mice resulted in progressive alopecia due to decreased stem cell activation (Li *et al*, 2012). However, variable and incomplete deletion of *Dnmt1* was seen in this conditional mouse model. We therefore used a different approach, epidermal DNMT1 ablation in immune competent mice using the Keratin 5-Cre (K5-Cre) system (Winter *et al*, 2013), to examine the effects of this loss on the skin.

Here, we show that DNMT1 ablation triggers a strong pathological innate immune response in the skin, resulting in immune cell infiltration and subsequent destruction of normal skin architecture. DNA hypomethylation in keratinocytes led to formation of micronuclei and accumulation of cytosolic DNA due to mitotic defects and genomic instability. This in turn caused cGAS-dependent activation of the innate immune system inducing an autoinflammatory phenotype. Intriguingly, additional deletion of cGAS in *Dnmt1*-deficient mice significantly diminished the innate immune response and significantly ameliorated the skin destruction phenotype. Our study reveals a novel role of DNA methylation in restraint of the innate immune response to self-nucleic acids.

Results

DNA hypomethylation results in disruption of epidermal homeostasis

To study the role of DNA methylation in epidermal morphogenesis and homeostasis, we deleted *Dnmt1* in mouse epidermis using *Keratin 5-Cre* (*K5-Cre*), which is active from embryonic day 9.5 (E9.5) (Ramirez *et al*, 2004). Mice examined had the following genotypes: *K5-Cre⁺ Dnmt1^{fl/fl}* (*Dnmt1^{Δ/Aep}*), *K5-Cre⁺ Dnmt1^{fl/+}* (*Dnmt1^{Δ/+ep}*), *Dnmt1^{fl/fl}* (control), and *Dnmt1^{fl/+}* (control). Immunolabeling of skin sections showed that Cre activation in *Dnmt1^{Δ/Aep}* mice resulted in loss of DNMT1 expression in all layers of the epidermis and in hair follicles, as well as greatly reduced 5-methylcytosine (5-mC) in these cells (Fig 1A and D). Strong DNMT1 staining remained evident in non-epithelial cells in the dermal layer (see also below). Analysis of mRNA and protein levels demonstrated that DNMT1 expression was strongly reduced in the epidermis of *Dnmt1^{Δ/Aep}* mice (Fig 1B and C). In accordance with data obtained with DNMT1-deficient embryonic stem cells (Li *et al*, 1992), deletion of *Dnmt1* in the epidermis resulted in a ~60% reduction in genome-wide DNA methylation in epidermal cells, as determined by quantitative HPLC (Fig 1E). Residual DNA methylation levels could be explained by DNMT1-positive immune cells migrating into the epidermis as well as by compensating activities of DNMT3A and DNMT3B (Tsumura *et al*, 2006).

Dnmt1^{Δ/Aep} mice were born at normal Mendelian ratios and initially displayed normal epidermal development, with regular barrier formation and unaffected differentiation (Appendix Fig S1A–C). However, from postnatal day 3 (P3) onward, *Dnmt1^{Δ/Aep}* mice developed a severe skin phenotype characterized by dry, reddish, scaly, and atrophied skin as well as by alopecia (Figs 1F and G, and EV1C and D). At later stages (P7–9), wounds and lesions appeared on mechanically challenged areas, such as the neck and the extremities (Fig 1F and G). Compared to control littermates, *Dnmt1^{Δ/Aep}*

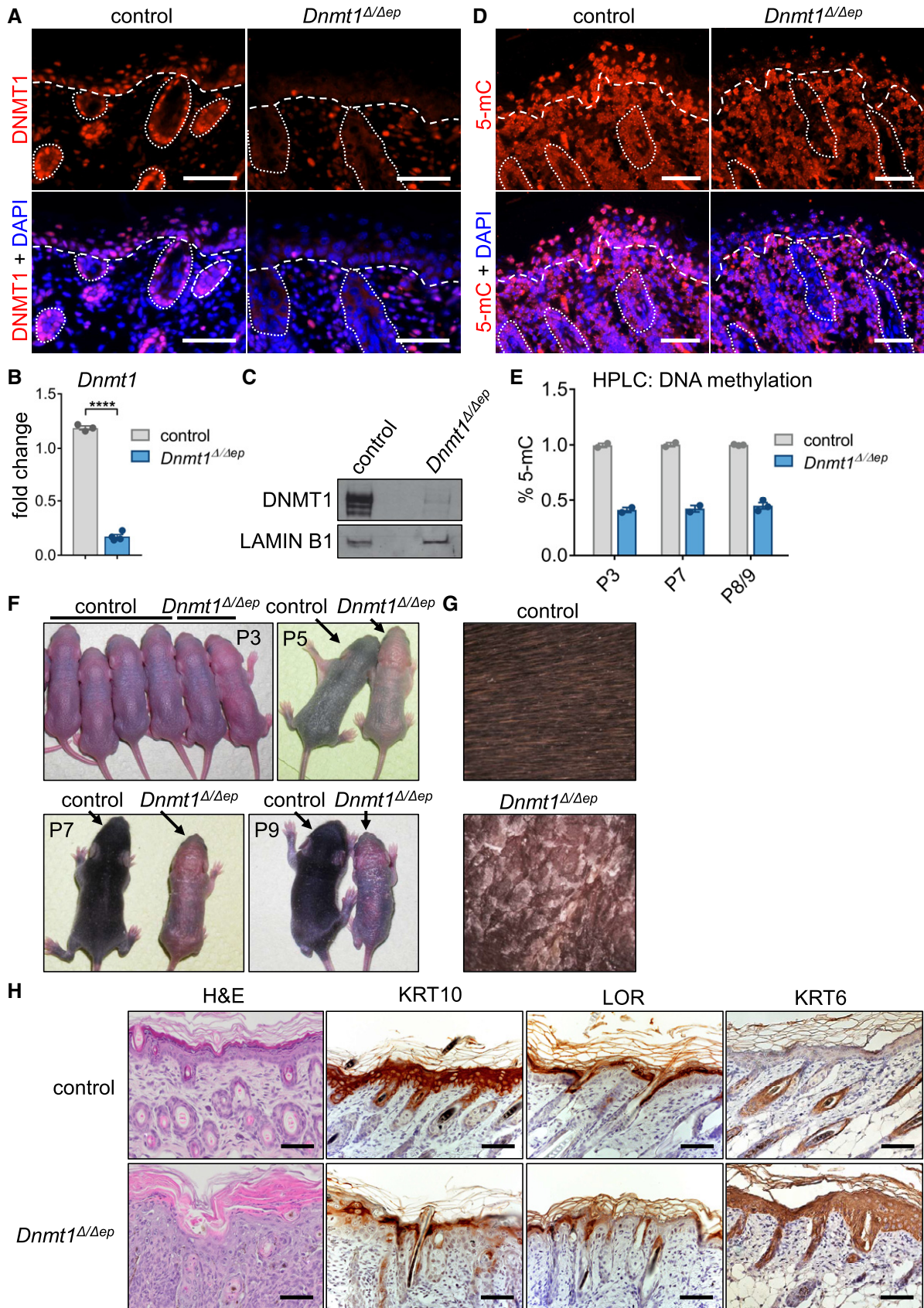


Figure 1.

Figure 1. Epidermal DNA hypomethylation results in a severe skin phenotype.

- A Immunofluorescence labeling of wild-type mouse dorsal skin samples (*Dnmt1^{fl/fl}* skin from P3) shows expression of DNMT1 throughout epidermal layers whereas keratinocyte-specific knockout (*Dnmt1^{Δ/Δep}*) results in the almost absence of a specific staining in the epidermis and in hair follicles. Dashed lines indicate the dermal–epidermal border, and dotted lines indicate hair follicles.
- B, C Deletion of DNMT1 was also confirmed in isolated epidermis by analysis of RNA expression ((B), and data are mean ± SEM, two-tailed *t*-test, *****p* ≤ 0.0001, *n* = 3–4 mice) and Western blotting (C).
- D Knockout of *Dnmt1* results in lower levels of DNA methylation in the epidermis and in hair follicles as determined by anti 5-mC labeling of P3 skin. Dashed lines indicate the dermal–epidermal border, and dotted lines indicate hair follicles.
- E HPLC analysis of cytosine methylation in the epidermis of *Dnmt1^{Δ/Δep}* mice compared with control littermates at different time points after birth. Values are percentages of methylated CpGs compared with total number of CpGs in the genome. P3: *n* = 2, P7: *n* = 2, P8/9: *n* = 3. Data are shown as mean ± SEM.
- F, G Images of control (*Dnmt1^{fl/fl}*, *Dnmt1^{fl/fl}*) and *Dnmt1^{Δ/Δep}* littermates at P3, P5, P7, and P9. An enlargement of the skin surface is shown on the right (G).
- H Hematoxylin and eosin (H&E) staining, immunolabeling for KERATIN 10 (KRT10), LORICRIN (LOR), and KERATIN 6 (KRT6) expression of dorsal skin sections (P5) of control and *Dnmt1^{Δ/Δep}* mice.
- Data information: Scale bars, 50 μm.

mice gained less weight until P6, lost weight thereafter, and died between P8 and P9 (Fig EV1A and B). The full milk belly of those pups indicates that abandonment or starvation was not the cause of death.

Histological examination revealed that these phenotypes in *Dnmt1^{Δ/Δep}* pups were underpinned by a prominent alteration in tissue architecture, characterized by dermal atrophy and massive infiltration of immune cells (Figs 1H and EV1C and D). The dermis showed mild to marked fibrosis, characterized by proliferating fibroblasts, increased numbers of fibrocytes and deposition of collagen, as determined by Azan staining (Fig EV1D). Within the epidermal compartment, we found acanthosis, hyperkeratosis, loss of keratohyalin granules, parakeratosis, and impaired keratinocyte differentiation, as shown by reduced levels of keratin 10 and loricrin (Figs 1H and EV1C).

The basal layer of the epidermis contains highly proliferative cells, which regularly exit the cell cycle and undergo terminal differentiation. Strikingly, cell proliferation was markedly enhanced in the epidermis of *Dnmt1^{Δ/Δep}* mice, with significantly more keratinocytes immunopositive for Ki67 and PCNA compared with control samples (Appendix Fig S2A–C). This was accompanied by dramatic upregulation of keratin 6, a marker for hyperproliferative, activated keratinocytes, found in wound healing (Fig 1H). In addition, we observed infiltration of inflammatory cells into the epidermis (exocytosis) with formation of micro-abscesses and crusts. Immunolabeling for p53 and for cleaved-caspase 3 revealed enhanced apoptosis in cells of the interfollicular epidermis and in hair follicles of P7 *Dnmt1^{Δ/Δep}* mice (Appendix Fig S2D and E). Furthermore, immunoblot analysis of epidermal isolates revealed induced DNA damage, indicated by the presence of gamma-H2A.X. (Appendix Fig S2F). Together, this analysis indicates that epidermal DNA hypomethylation induces a severe skin pathology.

Elevated innate immune response in the *Dnmt1^{Δ/Δep}* epidermis

Pathological assessment of skin histology suggests that disrupted epidermal homeostasis in *Dnmt1^{Δ/Δep}* mice is potentially the consequence of inflammatory disease. Thus, paraffin skin sections were immunolabeled for the presence of the common leukocyte antigen CD45. At P7, a massive increase in CD45-positive cells was observed in both the epidermis and the dermis of *Dnmt1^{Δ/Δep}* mice (Fig 2A). Although more leukocytes were found in all skin layers compared with control animals, immune cell infiltration was most obvious

within the papillary dermis, with the highest density of immune cells found toward the dermal/epidermal border (Fig EV2A). To determine the dynamics of immune cell infiltration, flow cytometric analysis was performed from skin specimens at different postnatal days. The proportion of CD45-positive cells in the epidermis and dermis increased over time in *Dnmt1^{Δ/Δep}* mice compared with control samples (Figs 2B and EV2B). The increase in immune cells is mainly due to the CD11b⁺ myeloid population. Further analysis of markers showed that these cells represent neutrophils (CD11b⁺ Ly6G⁺) and macrophages (CD11b⁺ F4/80⁺), whereas the percentage of antigen-presenting cells (LCs and DCs) remain largely unchanged (CD11b⁺ MHC-II⁺) (Figs 2C and EV2B). Consistent with an increase in CD11b⁺ cells, qRT–PCR analysis of selected chemokines revealed that *Ifng* and interferon-stimulated genes involved in innate immune responses, such as *Isg15*, *Cxcl1*, *Cxcl10*, *IL1b*, and *IL6*, were strongly induced in the epidermis, while *Tnfa* was moderately but significantly upregulated and *Ifna* was unchanged (Fig 2D). Furthermore, systemic effects such as reduced blood sugar levels, proteinuria, increased organ mass (liver and kidney), and reduced barrier function accompanied the immune phenotype and the early lethality of *Dnmt1^{Δ/Δep}* mice (Fig EV2C–F). These data suggest that *Dnmt1^{Δ/Δep}* mice mount a strong innate immune response in the absence of infection.

To investigate whether the effects of DNMT1 ablation in keratinocytes are cell-autonomous in the context of the innate immune response, RNA sequencing was performed using keratinocytes isolated from P3 *Dnmt1^{Δ/Δep}* and control mice. We found 1,339 genes up- and 114 genes downregulated in the absence of DNMT1 (abs(log2FC) < 1; *P* ≤ 0.05) (Dataset EV1). Using gene ontology analysis of the deregulated genes, we found enrichment of several pathways that are highly connected to inflammation, including immune response, defense response, or chemotaxis (Fig 2E). Upregulation of several immune genes such as *Ccr2* and *Oasl1* was confirmed by qRT–PCR (Fig 2F). Notably, the promoter regions of most of these genes, except for *Ccr2*, are hypomethylated in control keratinocytes, suggesting that their induction in *Dnmt1^{Δ/Δep}* keratinocytes is not a direct effect of local demethylation of regulatory regions in the absence of DNMT1 (Chatterjee et al., 2014) (Fig EV3A). With respect to proliferation, cultivated primary keratinocytes from *Dnmt1^{Δ/Δep}* mice behaved differently when compared to keratinocytes *in vivo*. *In vitro*, *Dnmt1^{Δ/Δep}* keratinocytes exhibited induction of the Cdk inhibitors *Cdkn2a* (*p16*) and *Cdkn2b* (*p15*) (Fig EV3B), while keratinocytes within the epidermis of *Dnmt1^{Δ/Δep}*

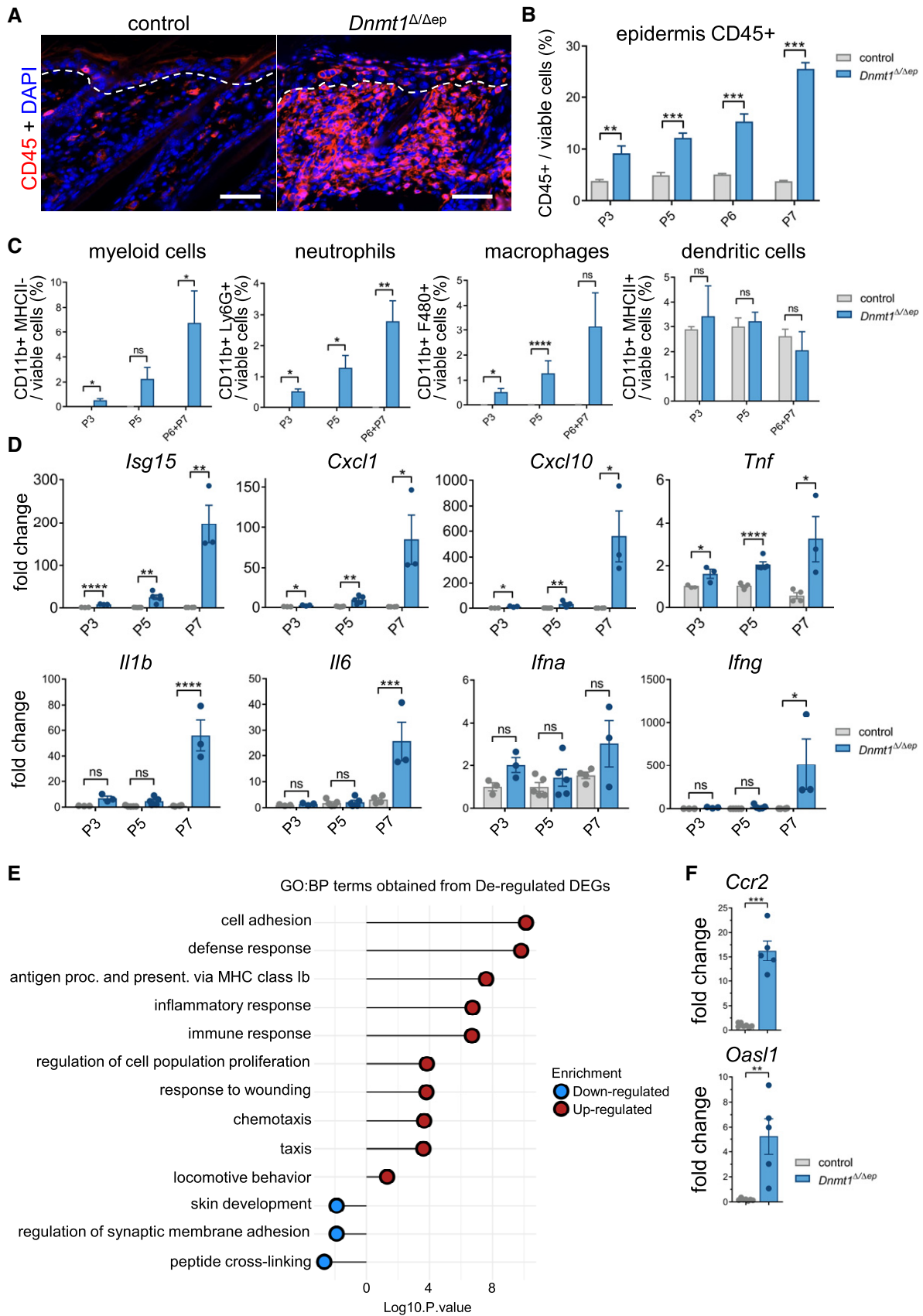


Figure 2.

Figure 2. Epidermal DNA hypomethylation results in induced immune response.

- A Representative immunostaining for CD45 of dorsal skin sections from control and *Dnmt1^{Δ/Δep}* mice at P7. Dashed lines indicate the dermal–epidermal border.
- B Flow cytometric analysis of CD45-positive cells isolated from the epidermis of control and *Dnmt1^{Δ/Δep}* mice of different postnatal ages. Cells are shown as percent of viable cells. Data are mean ± SD, two-tailed *t*-test, ***P* ≤ 0.01, ****P* ≤ 0.001, *n* ≥ 4 mice.
- C Flow cytometric analysis of the respective immune cell populations from the epidermis of control and *Dnmt1^{Δ/Δep}* mice of different postnatal ages. Cells are shown as percent of viable cells. Data are mean ± SEM, two-tailed *t*-test. ns, not significant, **P* ≤ 0.05, ***P* ≤ 0.01, *****P* ≤ 0.0001, *n* = 3 (P3), 4 (P5), and 4 (P6 + P7).
- D Relative mRNA expression levels of immune-related genes in control and *Dnmt1^{Δ/Δep}* mice at P3 (*n* = 3), P5 (*n* = 5), and P7 (*n* ≥ 3). Data are mean ± SEM. *P*-values are calculated using one-way ANOVA with post hoc Tukey multiple comparison test, **P* ≤ 0.05, ***P* ≤ 0.01, ****P* ≤ 0.001, *****P* ≤ 0.0001.
- E Gene ontology analysis of significantly up- and downregulated genes (*p*-value < 0.05) obtained from epidermal keratinocytes of control and *Dnmt1^{Δ/Δep}* mice (*n* = 3 mice). Keratinocytes were isolated from 3-day-old mice and cultured for 72 h.
- F Relative mRNA expression of representative immune-related genes found to be deregulated by RNA sequencing in keratinocytes cultured for 72 h and isolated from 3-day-old control and *Dnmt1^{Δ/Δep}* mice (*n* = 3 per group). Data are mean ± SEM, two-tailed *t*-test, ***P* ≤ 0.01; ****P* ≤ 0.001.

Data information: Scale bars, 50 μm.

mice showed hyperproliferation (Appendix Fig S2A–C). This difference emphasizes the importance of examining the role of DNA methylation in the *in vivo* context of a given tissue. In summary, these findings show that DNA hypomethylation in the epidermis induces a strong immune response in the skin.

The inflammatory phenotype of *Dnmt1^{Δ/Δep}* mice does not depend on MDA5/MAVS signaling

Previous studies have demonstrated that DNA-demethylating agents activate the innate immune system via the MDA5 (melanoma differentiation-associated protein 5) /MAVS (mitochondrial antiviral-signaling) RNA recognition pathway in tumor cells (Chiappinelli *et al*, 2015; Roulois *et al*, 2015). This RNA-sensing mechanism is induced by dsRNAs, which are in part derived from derepressed endogenous retroviral elements and its activation by viral mimicry was linked to the toxic effect of DNMT inhibitors on tumor cells (Licht, 2015). Analysis of transposon transcripts extracted from RNA sequencing data from *Dnmt1*-deficient keratinocytes revealed that different classes and families of transposons, in particular LTR retrotransposons, are upregulated (Dataset EV2 and Fig EV3C). As expected (Gaudet *et al*, 2004), strong, time-dependent activation of IAP (intracisternal A-type particle) LTR retrotransposons as well as of MLV retroviruses and LV30 transposons was observed by qRT–PCR analysis of epidermal samples from P0–P7 *Dnmt1^{Δ/Δep}* mice (Figs 3A and EV3C and D) and immunoblot analysis of the IAP Gag protein (Fig 3B). A similar increase in IAP transcript levels was also detected in cultivated keratinocytes from *Dnmt1^{Δ/Δep}* mice when compared to control samples (Fig EV3B). The increase in IAP transcripts was linked to reduced DNA methylation at IAP elements (Fig EV3E and F and Appendix Table S2). These data demonstrate that loss of DNMT1 in the epidermis results in DNA hypomethylation and derepression of transposons. Therefore, we examined whether activation of the MDA5/MAVS RNA recognition pathway is critical for the immune response and contributes to the skin phenotype observed in *Dnmt1^{Δ/Δep}* mice. We generated double knockout mice lacking DNMT1 and functional MAVS, the essential mediator of dsRNA recognition by MDA5. However, the histopathological phenotype including immune cell infiltration, as well as survival of the mice, was found to be similar to DNMT1 single knockout (Appendix Figs S3A–E and S4). To analyze whether additional ablation of MAVS has an influence on transcript levels of immune-related genes, qRT–PCR was performed from epidermal isolates of P7 mice. Most

immune genes analyzed showed a tendency toward reduced levels upon additional deletion of *Mavs* in the *Dnmt1^{Δ/Δep}* epidermis. However, with the exception of the chemokine *Ccr2*, none of these changes were statistically significant (Fig 3C). Taken together, these data indicate that induction of the innate immune system in the epidermis of *Dnmt1^{Δ/Δep}* mice is independent of transposon transcript recognition by the MDA5/MAVS pathway.

DNA hypomethylation induces the cGAS/STING pathway via cytoplasmic DNA

The *Dnmt1^{Δ/Δep}* epidermis displays increased DNA damage and apoptosis. Previous studies demonstrated that DNA hypomethylation in human colon cancer cells induced genomic instability and the formation of micronuclei (Stopper *et al*, 1993; Costa *et al*, 2016). To investigate whether epidermal cells of *Dnmt1^{Δ/Δep}* mice show similar nuclear aberrations, paraffin sections of the *Dnmt1^{Δ/Δep}* epidermis were stained with the ultra-sensitive DNA dye PicoGreen and microscopically evaluated. Epidermal *Dnmt1* deletion induced the formation of DNA blebs and micronuclei (Fig 4A). Importantly, these structures were not detected in the epidermis of control mice. Cytoplasmic double-stranded DNA originating from viruses or chromosomal instability in senescent or malignant cells is sensed by the cGAS/STING pathway, which in turn induces interferon-stimulated gene (ISG) expression (Dou *et al*, 2017; Gluck *et al*, 2017; Mackenzie *et al*, 2017; Bakhoun *et al*, 2018). In addition, the promoter region of the *Cgas* gene contains two adjacent IFN-sensitive response elements and different pattern recognition receptor ligands induce cGAS expression in an IFN-I-dependent manner, indicating that cGAS itself can be regarded as an ISG (Ma *et al*, 2015). Therefore, we analyzed the expression of cGAS protein in the epidermis and found substantially increased levels of cGAS in the *Dnmt1^{Δ/Δep}* epidermis compared with wild-type control both by immunolabeling and immunoblot analysis (Figs 4B and EV5B).

Next, we studied the relationship between DNMT1 inactivation and formation of micronuclei in *in vitro* cultured immortalized human keratinocytes. The drug 5-aza-2'-deoxycytidine (DAC) leads to DNMT inhibition and thus DNA hypomethylation (Stresemann & Lyko, 2008). Accordingly, DAC treatment of human keratinocytes for 72 h led to a reduction in protein levels of DNMT1 and the *de novo* methyltransferases DNMT3A and DNMT3B and reduced DNA methylation (Fig EV4D and E). Compared to control cells, DAC-treated keratinocytes generated significantly more micronuclei as

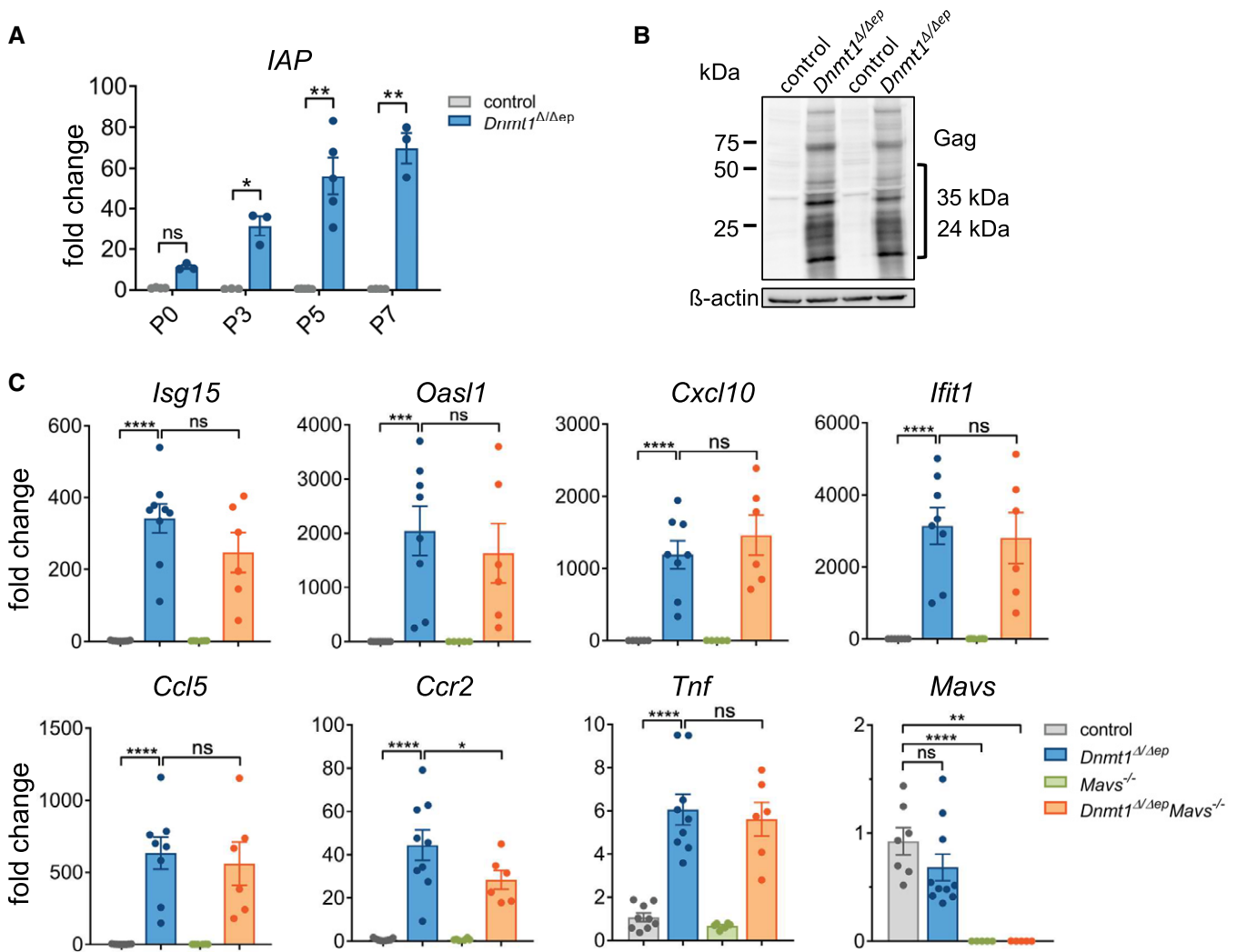


Figure 3. Epidermal deletion of DNMT1 results in derepression of transposable elements and activation of immune genes with minor impact of the MAVS pathway.

A Relative mRNA expression levels of epidermal Intracisternal A-type particles (IAPs) during different postnatal time points (P0 $n \geq 3$, P3 $n = 3$, P5 $n = 5$, P7 $n \geq 3$ mice), which were compared using one-way ANOVA with post hoc Tukey multiple comparison test. Data are mean \pm SEM. ns not significant, * $P \leq 0.05$, ** $P \leq 0.01$.
 B IAP protein was determined from epidermal isolates of two control and two *Dnmt1 Δ/Δ ep* mice. A bracket indicates the size of group-specific antigen (gag) proteins.
 C Relative expression of immune-related genes of the epidermis from P7 of control ($n \geq 7$), *Dnmt1 Δ/Δ ep* ($n \geq 8$), MAVS knockout (*Mavs $^{-/-}$* , $n = 7$), and *Dnmt1 Δ/Δ ep Mavs $^{-/-}$* ($n = 6$) mice was compared using one-way ANOVA with post hoc Holm–Sidak multiple comparison test. Data are mean \pm SEM. ns not significant, * $P \leq 0.05$, ** $P \leq 0.01$, *** $P \leq 0.001$, **** $P \leq 0.0001$.

shown by DNA labeling using PicoGreen (Fig 4C and D). Moreover, the majority of detected micronuclei recruited cGAS, as shown by double staining of DNA and anti-cGAS antibody (Fig 4E). Consistent with induction of an innate immune response, increased expression levels of the immune-related *CCL5* and *IFT2* were observed in DAC-treated keratinocytes (Fig 4F). DNA hypomethylation at pericentric chromosomal regions has been linked to defective mitosis, chromosome segregation errors, and chromosomal instability resulting in the formation of micronuclei, nuclear blebs, and nucleoplasmic bridges (Fenech et al, 2011; Costa et al, 2016). Indeed, visualization of mitotic chromosomes with an antibody specific for histone H3S10ph showed increased numbers of incomplete and disorganized mitosis in DAC-treated keratinocytes (Fig EV4F–H). In

particular, aberrant mitotic figures during telophase and nucleoplasmic bridges in post-mitotic cells were significantly elevated upon DAC treatment. Similarly, loss of *Dnmt1* led to DNA hypomethylation at pericentric repeats in murine keratinocytes (Fig EV3D and E). Analysis of H3S10ph-positive G2/M cells in the *Dnmt1 Δ/Δ ep* epidermis revealed a significant increase in G2/M cells in the suprabasal layers, which are normally devoid of G2/M cells as seen in control mice (Fig EV4A–C). Interestingly, the H3S10ph-positive G2/M cells in the suprabasal layers are negative for the proliferation marker Ki67, indicating that they are arrested in mitosis. Taken together, these findings suggest that loss of DNMT activity in keratinocytes induces chromosomal instability and disrupts cell cycle progression resulting in the formation of DNA blebs and

micronuclei. The detection of cytosolic DNA by cGAS induces a strong innate immune response in *Dnmt1^{Δ/Δep}* mice.

Deletion of cGAS ameliorates the autoimmune phenotype of *Dnmt1^{Δ/Δep}* mice

To examine whether cGAS/STING activation contributes to the autoinflammatory phenotype in response to DNA hypomethylation,

we treated primary keratinocytes with DAC and a novel STING inhibitor C-178 (Haag *et al*, 2018). DAC treatment of primary keratinocytes alone led to induction of immune genes including *Isg15*, *Oas1*, and *Ccl5* (Fig EV5A). Importantly, simultaneous treatment with the STING inhibitor C-178 resulted in significantly reduced activation of innate response genes. To further test the hypothesis that cGAS represents a critical mediator of pro-inflammatory signals in the hypomethylated epidermis, we generated *Dnmt1^{Δ/Δep} Cgas^{-/-}*

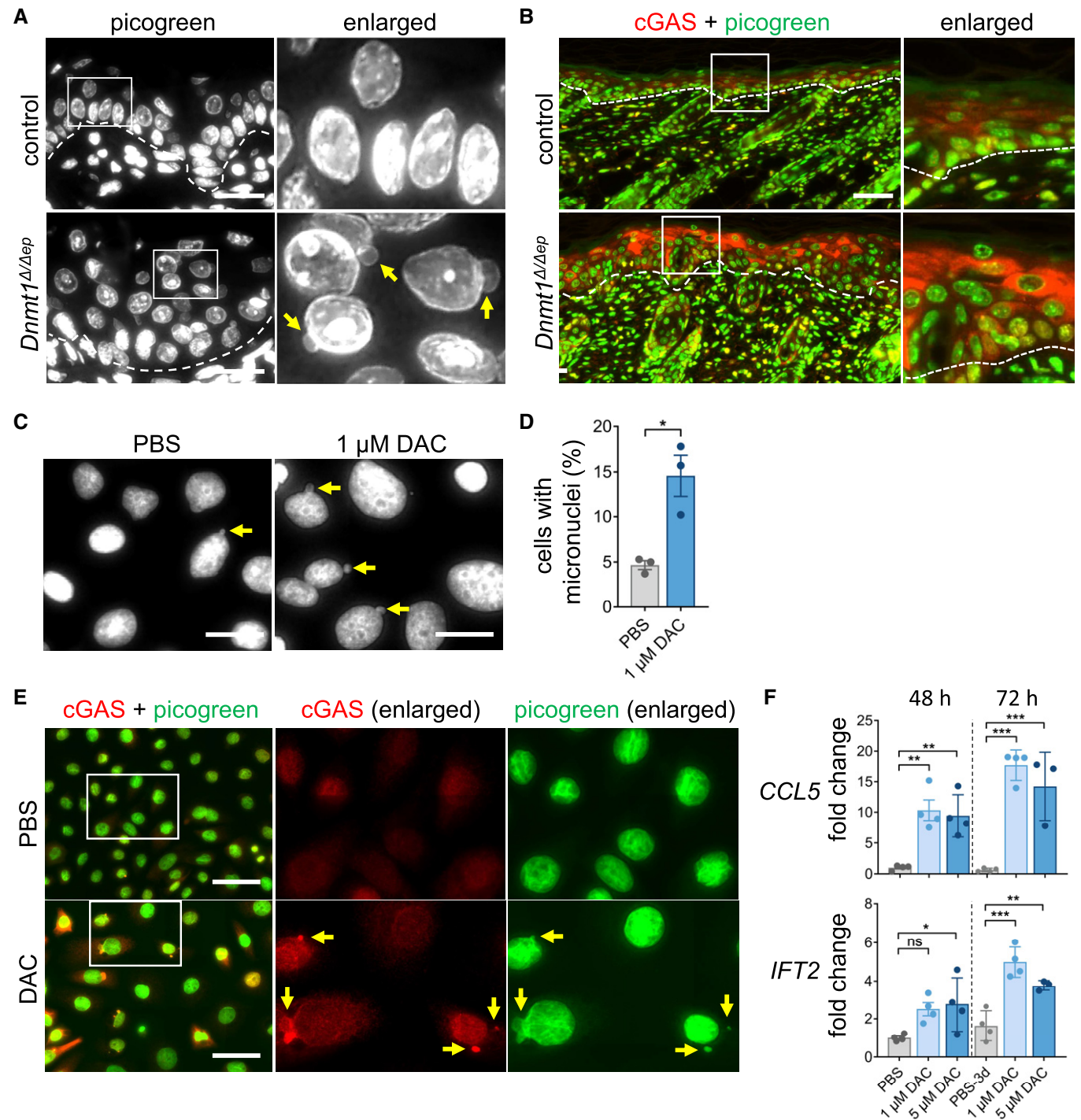


Figure 4.

Figure 4. DNA hypomethylation results in release of cytoplasmic DNA and cGAS activation.

- A Paraffin skin sections (P5) of control and *Dnmt1^{Δ/Δep}* mice were stained for DNA using PicoGreen. Enlarged sections are indicated on the right where arrows point to DNA-positive nuclear protrusions. Dashed lines indicate the dermal–epidermal border.
- B Labeling of dorsal skin sections of control and *Dnmt1^{Δ/Δep}* mice for cGAS and PicoGreen. Enlarged sections are indicated on the right. Dashed lines indicate the dermal–epidermal border.
- C–F Immortalized human keratinocytes (NHEK SV-Tert3-5) were treated with 5-aza-2'-deoxycytidine (DAC) or vehicle (PBS). (C, D) PicoGreen staining of PBS- and DAC-treated keratinocytes for 48 h detected micronuclei (arrow), which were analyzed in a blinded manner, and compared using two-tailed *t*-test. Data are mean ± SEM, **P* ≤ 0.05 (*n* = 3 biological replicates) (D). (E) Co-labeling of DNA by PicoGreen and by cGAS in PBS- and DAC-treated keratinocytes. Within enlarged sections on the right arrows point at DNA/cGAS double-positive blebs and micronuclei. (F) Relative expression of CCL5 and IFT2 in keratinocytes treated with PBS or DAC for 45 h or 72 h using one-way ANOVA with post hoc Dunnett multiple comparison test. Data are mean ± SEM. ns not significant, **P* ≤ 0.05, ***P* ≤ 0.01, ****P* ≤ 0.001 (*n* = 4 biological replicates).

Data information: Scale bars, 20 μm (A, D), 50 μm (B, E).

double knockout mice (Fig EV5B). The additional knockout of *Cgas* resulted in a significantly higher survival rate of mice when compared to *Dnmt1^{Δ/Δep}* mice (Fig EV5C). The severely impaired epidermal homeostasis observed in the *Dnmt1^{Δ/Δep}* mice before the full onset of an immune response suggests that DNMT1-dependent effects that are not linked to the innate immune response contribute to the lethal phenotype. This is also supported by the study of Sen *et al.* (Sen *et al.*, 2010) using a xenograft model with SCID mice. These immunocompromised mice show in the absence of DNMT1 severe epidermal defects independent of an activated immune system.

Importantly, histoscore of H&E-labeled paraffin skin sections revealed significant improvement of several histopathological parameters (Fig 5A and B, and Appendix Fig S4). Likewise, immune cell infiltration into the dermis and epidermis was strongly reduced upon additional deletion of *Cgas*, as shown by immunolabeling for CD45 (Fig 5C and D). To test, whether expression of immune-related genes reflected improvement of skin pathology in *Dnmt1^{Δ/Δep} Cgas^{-/-}*, epidermal isolates from P7 mice were analyzed. qRT-PCR revealed significant downregulation of interferon-stimulated genes (*Isg15*, *Ifit1*, *Oasl1*) and of chemokines and cytokines (*Ccr2*, *Ccl5*, *Cxcl10*) (Fig 5E). In agreement with previously published data (de Koning *et al.*, 2012), loss of epidermal DNMT1 resulted in a robust induction of AIM2 indicating a role of the inflammasome in the activation of the innate immune response. Interestingly, the AIM2 induction was largely dependent on the presence of cGAS supporting the idea of a cross-talk between the cGAS and the inflammasome as previously described (Swanson *et al.*, 2017). Taken together, these results indicate that activation of the innate immune system via the cGAS/STING pathway is a critical component of the inflammatory skin disease seen in *Dnmt1^{Δ/Δep}* mice.

Discussion

Our study reveals a crucial role for DNA methylation in epidermal homeostasis through both maintenance of genomic stability and prevention of inappropriate innate immune system activation. Mice with a *Keratin 5-Cre*-mediated deletion of *Dnmt1* show a normal epidermal development until birth. From P3 onwards, mice develop a severe skin phenotype characterized by disturbed epidermal homeostasis, and immune cell infiltration reflecting an excessive immune response. Sen *et al.* (Sen *et al.*, 2010) demonstrated that loss of DNMT1 in human keratinocytes resulted in impaired self-renewal and premature differentiation of epidermal progenitors.

Indeed, *in vitro* cultivated murine *Dnmt1*-deficient keratinocytes express increased levels of the senescence marker p15 and p16, reflecting in part the behavior of human DNMT1 knockdown keratinocytes (Sen *et al.*, 2010). In contrast, we observed hyperproliferation of keratinocytes in the epidermis of *Dnmt1^{Δ/Δep}* mice, which might be caused by the presence of immune cells and resident dermal cells, leading to mutual stimulation *in vivo* (Zheng *et al.*, 2007; Briso *et al.*, 2013). Another study using *Keratin 14-Cre* to delete *Dnmt1* in the epidermis reported reduced epidermal stem cell proliferation and hair germ formation in the absence of DNMT1 (Li *et al.*, 2012). These mice are viable, and their epidermis shows uneven thickness due to hyperproliferative regions. The changes in epidermal proliferation were interpreted as arising from a compensatory mechanism (Li *et al.*, 2012). Divergent results observed in these studies can be explained by differences in the origin of keratinocytes, the mouse models used, and the absence of immune cells in the xenograft model. The usage of an immunocompetent, conditional K5-cre mouse model allowed us to conduct a robust analysis of *Dnmt1* deletion in the skin.

Several reports have implicated DNMT1 in the regulation of mammalian cell fate decisions in different tissues and organs. *Dnmt1* deletion during embryogenesis caused an acute phenotype of the intestine, characterized by weight loss, global DNA hypomethylation, genome instability, apoptosis, and loss of nascent villi (Elliott *et al.*, 2015) (mitotic genes were top hits among downregulated genes). In the mature intestinal epithelium, DNMT1 controls cellular differentiation, but is dispensable for organ maintenance and organismal survival in adult mice (Sheaffer *et al.*, 2014). In the nervous system, DNMT1 has been shown to be essential for survival of fetal mitotic neuroblasts. Mice with *Nestin-Cre*-mediated deletion of *Dnmt1* die after birth due to respiratory defects (Fan *et al.*, 2001). In the pancreas, ablation of DNMT1 results in a decrease in differentiated pancreatic cells with a concomitant increase in p53 levels, cell cycle arrest, and progenitor cell apoptosis (Georgia *et al.*, 2013). Taken together, all these studies indicate a regulatory role of DNMT1 in the control of progenitor self-renewal and differentiation. The present study links tissue-specific loss of DNMT1 to innate immune system activation and systemic defects, providing a holistic view of the impact of deregulated DNA methylation at the organismal level.

We here report for the first time that autoinflammation of the skin is a direct consequence of DNMT1 ablation *in vivo*. DNA hypomethylation in the epidermis results in the activation of the innate immune system, likely linked to the skin's unique function as an immune organ consisting of highly proliferating basal

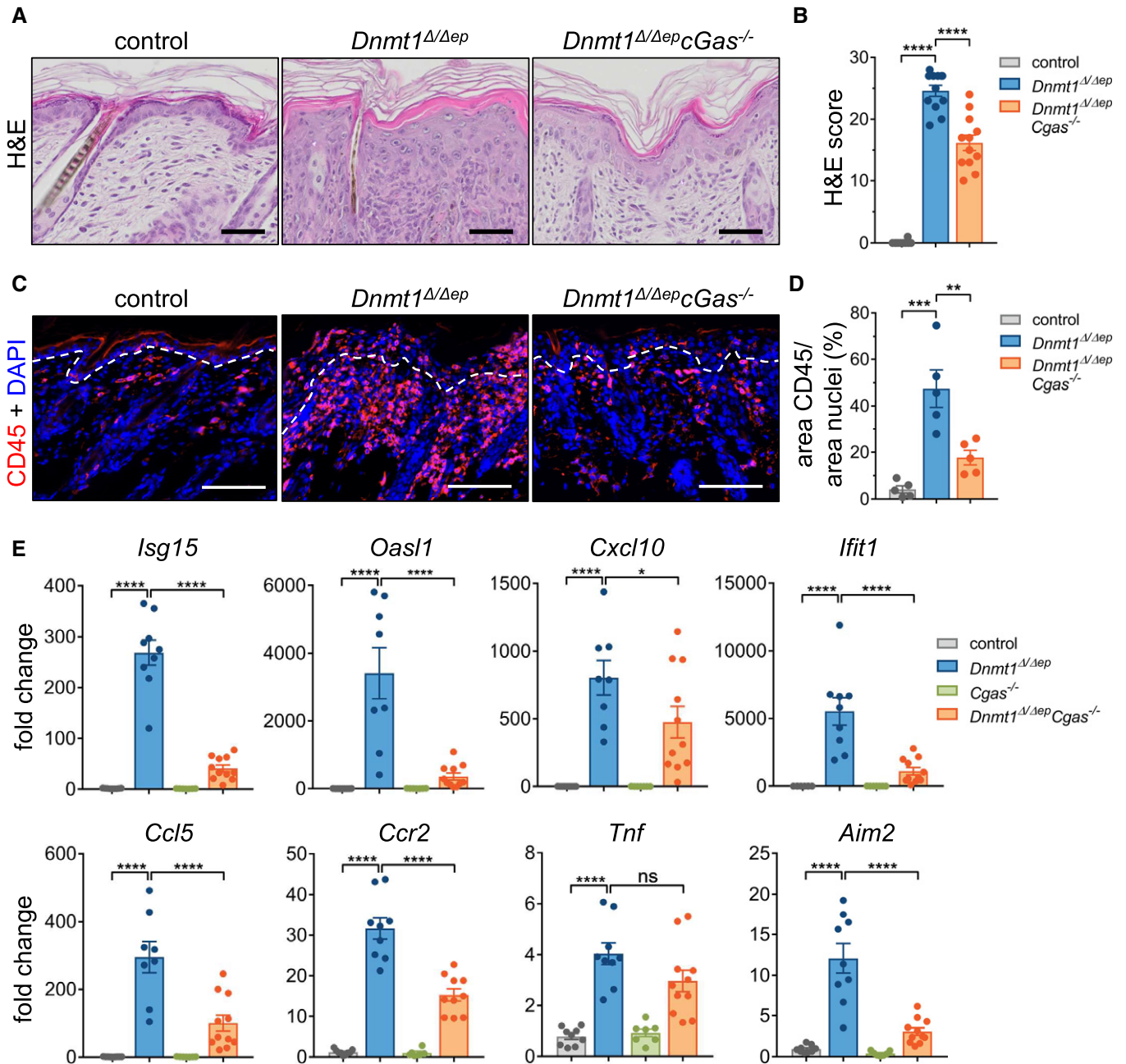


Figure 5. Additional deletion of cGAS attenuates the autoinflammatory *Dnmt1*^{Δ/Δep} skin phenotype.

A Representative images of P7 H&E-labeled dorsal skin sections of control (*Dnmt1*^{fl/fl}), *Dnmt1*^{Δ/Δep}, and *Dnmt1*^{Δ/Δep} *Cgas*^{-/-} mice.

B The histopathology of at least 9 animals per genotype was assessed in a blinded manner, and an overall score was determined from individual parameters (see Appendix Fig 7 and Appendix Table S3). Comparison was performed using one-way ANOVA with post hoc Holm–Sidak multiple comparison test. Data are mean ± SEM. *****P* ≤ 0.0001.

C Representative images of CD45 immunofluorescence labeling of P7 dorsal skin sections from *Dnmt1*^{fl/fl}, *Dnmt1*^{Δ/Δep}, and *Dnmt1*^{Δ/Δep} *Cgas*^{-/-} mice. Dashed lines indicate the dermal–epidermal border.

D Quantification of CD45-positive cells. Tissue sections approximately 1 cm in length were scanned, and the area of CD45-positive cells per area of nuclei was quantified using ImageJ. Sections obtained from five mice per genotype were analyzed, and calculated values were compared using one-way ANOVA with post hoc Holm–Sidak multiple comparison test. Data are mean ± SEM. ***P* ≤ 0.01, ****P* ≤ 0.001.

E Epidermis obtained from P7 control, *Dnmt1*^{Δ/Δep}, *Cgas*^{-/-}, and *Dnmt1*^{Δ/Δep} *Cgas*^{-/-} mice was analyzed for relative mRNA expression levels of immune-related genes using one-way ANOVA with post hoc Holm–Sidak multiple comparison test. Data are mean ± SEM. ns not significant, **P* ≤ 0.05, *****P* ≤ 0.0001. At least 7 mice per genotype were used.

Data information: Scale bars, 50 μm (A), 100 μm (C).

keratinocytes and skin-resident and infiltrating immune cells (Kaba-shima *et al*, 2019; Nguyen & Soulika, 2019). We find that *Dnmt1^{A/Aep}* mice show an elevated innate immune response in the epidermis, immune cell infiltration in the skin, and systemic effects in response to inflammation. *In vitro* experiments with keratinocytes demonstrated that the elevated expression of immune genes in response to DNA hypomethylation is at least in part a cell-intrinsic effect. Our data demonstrate that DNMT1 loss in the epidermis induces aberrant changes in cellular nucleic acid abundance and localization, triggering a strong innate immune response.

In accordance with previous reports on other cell types (Fan *et al*, 2001; Gaudet *et al*, 2004; Georgia *et al*, 2013), the *Dnmt1^{A/Aep}* epidermis displays a dramatic increase in the expression of IAPs and other transposons. An RNA-dependent immune response to DNA hypomethylation was previously reported for human tumor cells upon treatment with DNMT inhibitor (Chiappinelli *et al*, 2015; Roulois *et al*, 2015). In this setting, the MDA5/MAVS pathway is activated in response to retrotransposon-derived double-stranded RNA. In a follow-up study, it was shown that upon inhibition of DNA methylation, intronic and intergenic SINES activate MDA5 in cancer cells in an ADAR1-dependent manner (Mehdipour *et al*, 2020). Accordingly, loss of the RNA-editing enzyme ADAR1 causes an enhanced interferon response and embryonic lethality, which is rescued by additional *Mavs* knockout (Mannion *et al*, 2014). In the context of epidermal DNA hypomethylation, we did not detect a significant contribution of MDA5/MAVS signaling to the observed phenotypes. It remains possible that transposon activation contributes to the immune phenotype of *Dnmt1^{A/Aep}* mice. LINE1 retrotransposon activation in response to depletion of the histone deacetylase SIRT6 leads to accumulation of cytoplasmic L1 cDNA, which triggers a strong type I interferon response via cGAS activation (Simon *et al*, 2019). Future work will test whether other nucleic acid-sensing mechanisms are activated by (reverse) transcription of mobile elements.

A hallmark of *Dnmt1*-deficient or 5-aza-2'-deoxycytidine-treated keratinocytes in our study is incomplete or defective mitosis resulting in the presence of cytosolic DNA, detected as blebs, micronuclei and nucleoplasmic bridges. DNA hypomethylation has been previously shown to induce genomic instability, DNA damage, and mitotic arrest in human cancer cells (Chen *et al*, 2007; Costa *et al*, 2016), and in combination with Poly(ADP ribose) polymerase inhibition, it causes inflammation and reduced DNA repair (McLaughlin *et al*, 2020). In macrophages, DNMT3A induces HDAC9 to deacetylate TBK1 for activation of antiviral innate immunity (Li *et al*, 2016). Mutations in the human DNMT3B gene result in ICF (immunodeficiency, centromeric region instability, and facial anomalies syndrome) (Xu *et al*, 1999). ICF patient cells show genomic instability highlighted by the presence of micronuclei and nuclear blebs. Our findings further highlight a crucial function for DNA methylation in the maintenance of chromosomal stability. Cytosolic DNA in the *Dnmt1^{A/Aep}* epidermis and 5-aza-C-treated keratinocytes was recognized by cGAS, resulting in upregulation of the DNA-sensor protein by feedback. Ablation of cGAS in *Dnmt1^{A/Aep}* mice significantly attenuated the activation of immune genes, infiltration of immune cells, and destruction of the skin architecture suggesting a major contribution of the cGAS/STING pathway to the autoinflammatory phenotype of *Dnmt1^{A/Aep}* mice. Mice deficient in the DNA exonuclease *Trex1* develop systemic inflammation (Morita

et al, 2004) ameliorated by simultaneous deficiency in STING or cGAS (Gray *et al*, 2015). Similarly, deletion of *Cgas* or *Sting* in mice lacking DNase II, a lysosomal enzyme that digests DNA, rescued the lethal autoimmune phenotypes of the DNase II knockout mice (Ahn *et al*, 2012; Gao *et al*, 2015). Taken together, DNA-modifying and processing enzymes prevent the accumulation of cytosolic DNA and thereby the unwanted activation of the innate immune system by self DNA.

Additional loss of cGAS does not fully abolish the autoinflammatory phenotype of *Dnmt1^{A/Aep}* mice. It is conceivable that other pathways of the innate immune system such as TLR3 (dsRNA), TLR2/TLR4 (protein), the inflammasome (DNA, RNA, protein), TLR9 (hypomethylated ssDNA, RNA/DNA hybrids), or ZBP1 (Z-DNA, Z-RNA) are also induced in the epidermis of these mice (Kawai & Akira, 2011; Rigby *et al*, 2014; Bartok & Hartmann, 2020; Devos *et al*, 2020; Jiao *et al*, 2020). Gene mutations resulting in defective DNA/RNA modification and turnover pathways are associated with autoinflammatory diseases (Uggenti *et al*, 2019; Bartok & Hartmann, 2020; Melki & Fremond, 2020). In addition to genetic factors, also epigenetic dysregulation contributes to the development of pathogenesis (Alvarez-Errico *et al*, 2017). Therefore, it will be interesting to investigate whether changes in epigenetic patterns and nucleic acid-sensing mechanisms in the skin also contribute to autoinflammatory disorders.

The data presented here have potential implications for cancer treatment. cGAS/STING agonists have been considered as promising therapeutics in combination with immune checkpoint inhibitors in particular (Flood *et al*, 2019; Hoong *et al*, 2020). Current efforts to advance immunotherapy focus on testing drug combinations involving epigenetic drugs, which stimulate both innate and adaptive immune responses (Jones *et al*, 2019; Hogg *et al*, 2020) (Daver *et al*, 2018; Lai *et al*, 2021). Our study indicates that in addition to activation of RNA-sensing pathways *via* derepression of mobile elements, DNMT inhibitors could be used to trigger the controlled activation of the immune system through DNA-sensing pathways. Both processes might contribute to an increased efficacy of a combination of epigenetic and immune checkpoint therapies in tumor treatment.

Materials and Methods

Animal care, transgenic mouse lines, and mouse experiments

All mouse lines were bred to a mixed genetic background of C57BL/6J 129SV. *Keratin 5-Cre (K5-Cre)* mice (Ramirez *et al*, 2004) were mated to *Dnmt1^{fl/fl}* (Jackson-Grusby *et al*, 2001; Lee *et al*, 2001), *Mavs^{-/-}* (Sun *et al*, 2006), and *Cgas^{-/-}* (Schoggins *et al*, 2014) mice to generate mice with deletions of *Dnmt1* in the epidermis or epidermal *Dnmt1*, *Mavs*, and *Cgas*, respectively. Mice were kept in the animal facilities of the Medical University of Vienna in accordance with institutional policies and federal guidelines. All animal experiments were performed in accordance with a protocol authorized by the Austrian Ministry of Science and Research, following the approval by the National Ethical Committee for Animal Experimentation. The Austrian Ministry for Science and Research approved the corresponding proposals GZ BMWFV-66.009/0138-WF/V/3b/2017 and GZ BMWFV-66.009/0276-WF/V/3b/2017.

Genotyping primer

K5-Cre forward and reverse (TAA TCG CCA TCT TCC AGC AG and CAA TTT ACT GAC CGT ACA C), *Dnmt1 flox* forward and reverse (AAC CGT TGG CTT TTT GAG TGA G and AGA AAT AAA AAG CCA GTT GTG T), *Cgas* forward, reverse 1, reverse 2 (ATA TTT CCC CCT GTG TTG GA, GTG CCA GGT GAC ACA ACA TC, CGG ATG GAT GAA CAA ACA GA), *Mavs 1, 2, 3* (AGC CAA GAT TCT AGA AGC TGA GAA, TAG CTG TGA GGC AGG ACA GGT AAG G and GTG GAA TGT GTG CGA GGC CAG AGG C).

For the dye exclusion assay, embryos (E19.5) were killed and incubated for 1 min in 25, 50, and 75% methanol in PBS, followed by a 1-min incubation in 100% methanol, and a descending series of incubations in 75, 50, and 25% methanol in PBS for 1 min. Pups were washed in PBS and stained with 0.1% toluidine blue O (Sigma) for 1 min. Destaining was done in PBS. Blue-stained navel served as positive control for successful staining.

Dehydration assay was performed to measure the extent of fluid loss during a certain time frame and reflects the dysfunction of the skin barrier. Pups were separated from their parents on the indicated postnatal day (P3-P9) and kept at 37°C in the incubator for 6 h. Their weight was measured every 30 min, and weight loss was calculated as a function of time in relation to the starting weight of the pups (Leyvraz *et al*, 2005).

Blood sugar was monitored with a glucose meter. Spontaneous urine was collected and analyzed with the pyrogallol red-molybdate method, according to Fujita *et al*. performed by the company In Vitro Laboratory for veterinary Diagnostics and Hygiene GmbH Vienna, Austria.

Epidermis isolation and keratinocyte culture

Murine skin was isolated and incubated with the dermis side in PBS containing 5 mg/ml Dispase (Roche) for 2 h, at 4°C for protein and RNA isolation and at 37°C for keratinocyte isolation. Epidermis was removed from dermis, washed in PBS, and snap-frozen for protein and RNA analysis. In case of RNA isolation, solutions were supplemented with RNase Inhibitor (Winter *et al*, 2013). Mouse epidermal keratinocytes were isolated as previously described (Sibilia *et al*, 2000) and cultured in keratinocyte growth medium (KGM Gold BulletKit, Lonza) containing 8% chelated fetal calf serum and 0.05 mM CaCl₂ on collagen-fibronectin-coated dishes. Immortalized human epidermal keratinocytes NHEK/SVTERT3-5 (Wagner *et al*, 2018) (EVERCYTE, Vienna, Austria, CLHT-011-0026-5) were grown in KGM2 (C-20011, PromoCell) adjusted to 0.06 mM CaCl₂ and propagated according to the manufacturer's instruction.

Treatment and immunofluorescence (IF) analysis of keratinocytes

Cells were seeded either onto glass coverslips (for IF) placed in 6-well plates or into 12-well plates (for RNA expression analyses) one day before treatment. On the next day, cells were treated with either the vehicle control PBS or the DNMT1 inhibitor 5-Aza-2'-deoxycytidine (DAC; Sigma-Aldrich). To inhibit the cGas/Sting pathway, the cells were treated with the inhibitor C-178 (generous gift from Andrea Ablasser (Haag *et al*, 2018)) 24 h after the first DAC treatment. Keratinocytes were harvested either 24 h (IF) or 48 h (IF, RNA) after DAC

treatment. For IF analysis, cells were washed in ice-cold PBS, fixed in 4% paraformaldehyde for 20 min at 4°C, washed with PBS, and stored at 4°C until further analysis. For IF, cells were permeabilized using 0.1% Triton X in PBS for 20 min at room temperature than blocked in 2% BSA in PBS with 10% goat serum for 30 min at room temperature. Antibodies specific for human cGAS (#D1D3G, Cell signaling Technology, 1:200) and ph-Histone Histone H3, Ser 10 (SC-8658-R, Santa Cruz Biotechnology, 1:2,000) were overnight incubated at 4°C. After washing three times with PBS containing 0.1% Tween-20, the coverslip sections were incubated with Alexa Fluor 546-conjugated secondary antibody (Fisher Scientific) for 1 h at room temperature. After washing three times with PBS containing 0.1% Tween-20, the samples were counterstained with 1 µg/ml 4',6-diamidino-2-phenylindol (DAPI, Sigma-Aldrich) and PicoGreen dsDNA Reagent (Fisher Scientific, 1:2,000) for 20 min in TE buffer (10 mM Tris-HCl, 1 mM EDTA, pH 8.0). Coverslips were subsequently washed 3 times in PBS and mounted on SuperFrost Plus Adhesion slides (Thermo Scientific) using ProLong Gold (Thermo Fisher Scientific).

Determination of chromosomal aberrations during mitosis

Human keratinocytes treated with DAC for 24 or 48 h were immunolabeled for histone H3S10ph and counterstained with PicoGreen. About 100 mitotic H3S10ph-positive nuclei were analyzed in a blinded and randomized manner, classified into mitotic phases, and assessed for chromosomal aberrations.

Hematoxylin and eosin (H&E) labeling, immunohistochemistry (IHC), immunofluorescence (IF), and TUNEL analyses

Tissue samples were fixed overnight in 4% PFA and further embedded in paraffin. Stainings were performed on 4-µm sections using SuperFrost Plus Adhesion slides (Thermo Scientific). H&E stainings were carried out according to the standard procedure with a COT 20 Linear Slide Stainer (Meditate). IF and IHC analyses were carried out according to protocols published previously (Fischer *et al*, 2005) with modifications. Briefly, paraffin sections were prepared for staining by heat antigen retrieval using a pressure cooker (2100 Antigen Retriever, Aptum Biologics) for 20 min at 121°C. Depending on the used antibody, the slides were cooked in 10 mM Citrate buffer (pH 6) or in Dako Target Retrieval Solution (pH 9; Agilent). Samples were cooled down and incubated with phosphate-buffered saline, pH 7.2, plus 2% BSA and plus 10% goat serum (DAKO) for 20 min to block nonspecific binding. The slides were incubated overnight at 4°C using a humid chamber. For IHC, samples were incubated with the respective secondary antibody, stainings were visualized with the VECTASTAIN ABC kit and DAB substrate (Vector labs) and sections were counterstained with hematoxylin. For IF, sections were incubated with the appropriate Alexa Fluor 488/546-conjugated secondary and counterstained with 1 µg/ml 4',6-diamidino-2-phenylindol (DAPI, Sigma-Aldrich) and PicoGreen dsDNA Reagent (Fisher Scientific, 1:2,000) for 20 min in TE buffer (10 mM Tris-HCl, 1 mM EDTA, pH 8.0). The slides were mounted with Prolong Gold (Thermo Fisher Scientific). For *in situ* labeling of 3'-OH ends of DNA, the TUNEL assay (Roche) was performed according to the manufacturer's instructions (Fischer *et al*, 2005).

Primary antibodies used for IHC

Ki67 (1:500, Novocastra), Keratin 10, Keratin 6, Loricrin (1:1,000, Covance), p53 (1:50, NCL-p53-CM5p, Novocastra), cleaved-caspase 3 (1:200, CC3, cs-96615, Cell Signaling), PCNA (1:200, DAKO), DNMT1 (1:200, Abcam, ab188453), CGAS (1:100 Cell Signaling, 31659; 1:200 Cell Signaling 15102) 5 mC (1:500, Diagenode 006-500), CD45 (1:1,000, Abcam ab10558), and histone H3S10ph (1:2,000, Santa Cruz Biotechnology SC-8656-R).

Microscopy, image processing, and image analysis

H&E, IHC, and immunolabeling were analyzed using a slide scanner (VS120 S6, Olympus) equipped with a XM10 monochrome camera (Olympus) and a Pike F-505C color camera (Allied Vision). Image scans were obtained and further processed using the following Programs: VS-ASW 2.9, OlyVia (Olympus) and Adobe Photoshop CS6 (Adobe). For some IF analyzes, images were taken using a LSM Meta 510 confocal microscope (Zeiss). It was ensured that identical exposure times and gray value settings were used for the samples to be compared. For automated image quantification, a script was developed using Fiji software (Schindelin *et al*, 2012). In brief, a tissue mask was interactively created corresponding to the tissue region of interest. Particle analysis was done after applying a fix threshold to allow a comparative analysis. For enhanced particle separation, a watershed algorithm was used. Particle analysis revealed the parameters particle count, area, and area fraction of the tissue region of interest. For the quantification of Ki67, positive cells in the interfollicular epidermis (IFE), positive cells of the basal, and suprabasal layers of the IFE were counted and set in relation to the total cell number.

Histopathology

Paraffin sections of back skin which were stained by H&E and by azan were scanned using a slide scanner (VS120 S6, Olympus) equipped with 40x objective and a Pike F-505C color camera (Allied Vision). Scanned images were analyzed by a certified pathologist in a blinded manner using the OlyVia software (Olympus). Samples were scored for nine pathological alterations and graded from 0 to 5. For details of analyzed alterations and grading system, see Appendix Fig S4 and Appendix Table S1. All scores were summed up, and total H&E score is given in the figure.

Quantification of 5-methylcytosine (5-mC)

For 5-mC quantification in the mouse epidermis, genomic DNA was extracted using the phenol/chloroform method. Briefly, mouse epidermis (as isolated described above) was incubated overnight in 4.5 ml proteinase K buffer with 300 μ l proteinase K (20 mg/ml, 50 mM Tris-HCl pH8.0, 100 mM NaCl) and 250 μ l SDS at 55°C. Then, 200 μ l of 5 M NaCl and 5 ml phenol/chloroform were added. This was vortexed for 30 sec and then centrifuged for 5 min at 1,150 g at 4°C. The aqueous phase was subsequently transferred to a new tube, and 5 ml of chloroform was added. This was vortexed and centrifuged again, and the aqueous phase was put into a fresh tube. Three volumes of 96% ethanol were added, and DNA was then fished out with a glass hook, was centrifuged again, and washed in 70% ethanol. After drying the pellet, it was

resuspended and dissolved in 400 μ l TE buffer (1 M Tris-HCl pH 8.0, 0.5 M EDTA) for 5 min at 65°C. HPLC analysis of isolated DNA was performed as previously described (Ramsahoye, 2002). Genomic methylation was assessed by measuring methyl group carrying and unmodified cytidine nucleotides. HPLC shows the percentage of deoxy-methyl-cytidine-mono-phosphate (dmCMP) from total cytidines (dmCMP and dCMP). For 5-mC quantification in human keratinocytes, DNA methylation was analyzed by quantitative dot blot analysis as previously described (Zupkovitz *et al*, 2021).

DNA methylation analysis of selected repetitive elements

Epidermis of P7 mice was prepared by treatment with Dispase II solution (5 mg/ml in 1x PBS; Roche) for 45 min, 37°C. Epidermal cells were isolated by shaking in DNase I solution containing 250 μ g/ml DNase I (DN25, Sigma-Aldrich), 8% chelated fetal bovine serum (F2524, Sigma-Aldrich) in MEM (Sigma-Aldrich) for 30 min at 37°C. After filtration using a 70- μ m cell strainer, CD45-positive cells were depleted using Mojosort Mouse CD45 Nano-beads (480027, BioLegend) according to manufacturer's instructions. Purity of epidermal keratinocytes was checked by flow cytometry using anti-CD45. Genomic DNA of keratinocytes was prepared using Genelute Mammalian Genomic DNA Kit (G1N70 Sigma-Aldrich). DNA methylation status of selected repetitive elements was analyzed using deep amplicon bisulfite sequencing (IAP-LTR1a) or deep hairpin-bisulfite sequencing (major Satellites) according to Arand *et al*, 2012 (Arand *et al*, 2012), with slight modifications. Briefly, after bisulfite conversion, DNA was bound to MagBinding Beads (Zymo Research) in 7 M guanidine-HCl buffer. After washing with 80% EtOH in 10 mM Tris-HCl pH 8.0, DNA was desulfonated using 0.1 M NaOH in 70% isopropanol followed by two washes with 80% EtOH in 10 mM Tris-HCl pH 8.0 and elution in water. Amplicons were amplified using fusion primers of the repeat-specific primer and part of the TruSeq adaptor sequence. A second amplification step with six cycles was performed using full TruSeq adaptor sequences involving custom dual-index barcodes. Analysis for IAP-LTR1a (specific primer sequences: GAT AGT TGT GTT TTA AGT GGT AAA TAA A and TCC CTA TTA AAA AAA ATT ATC CTT C) omitted restriction and ligation reaction before bisulfite treatment. After equimolar pooling of purified amplicons, the library was sequenced on a MiSeq nano 2 \times 150 bp run. Reads were demultiplexed and trimmed for adaptor sequences using cutadapt v2.10 (Martin, 2011). Paired reads were merged using flash (Magoc & Salzberg, 2011), and different amplicons were separated using cutadapt v2.10 by primer sequence. CpG methylation was determined using BiQAnalyzerHT (Lutsik *et al*, 2011) according to Arand *et al* (2012). More than 1,300 reads were obtained for every sample, with an average conversion rate of 99.5% as determined from the Hairpin adaptor sequence (see Appendix Table S2).

DNA methylation profile at selected genes upregulated in *Dnmt1^{Δ/Δep}* mice

DNA methylation status of the genomic loci of immune genes derived from wild-type keratinocytes was obtained from Chatterjee *et al*, 2014 (Chatterjee *et al*, 2014) and visualized in IGV browser

(<http://software.broadinstitute.org/software/igv/home>), Broad Institute and UC San Diego, CA.

RNA isolation and real-time PCR analysis

Total RNA was isolated following the manufacturer's instructions (TRIzol, Invitrogen). RNA was reversely transcribed with the iScript cDNA Synthesis Kit (Bio-Rad). Real-time PCR analysis was performed with the KAPA SYBR FAST qPCR MasterMix (Peqlab) on an iCycler IQ system (Bio-Rad). Relative expression levels were normalized to HPRT (mouse) or *B2 M* (human).

qPCR primer for mRNA expression of mouse genes

Hprt forward (5') and reverse (3') (GCTGGTGAAAAGGACCTCT and CACAGGACTAGAACACCTGC *Cxcl1* forward and reverse (CTG CAC CCA AAC CGA AGT C and AGC TTC AGG GTC AAG GCA AG); *Cxcl10* forward and reverse (TTC TGC CTT CAT CCT GCT G and AGA CAT CTC TGC TCA TCA TTC); *Cldn1* forward and reverse (CTT CTC TGG GAT GGA TCG and GGG TTG CCT GCA AAG TAC TGT); *Cldn3* forward and reverse (GCG GCT CTG CTC ACC TTA GT and GAC GTA GTC CTT GCG GTC GTA); *Cldn8* forward and reverse (TCA GAA TGC AGT GCA AGG TC and AGC CGG TGA TGA AGA AGA TG); *Cdkn2a* forward and reverse (GAA CTC TTT CGG TCG TAC CCC and CAG TTC GAA TCT GCA CCG TAG); *Cdkn2b* forward and reverse (CCC TGC CAC CCT TAC CAG A and CCC TGC CAC CCT TAC CAG A); *Isg15* forward and reverse (AAG CAG ACT CCT TAA TTC C and CTG TAC CAC TAG CAT CAC); *Tnf* forward and reverse (CAG GAG GGA GAA CAG AAA C and ACA AGC AGG AAT GAG AAG AG); *Oasl1* forward and reverse (ACC AGC AGT ATG TGA GAG and GGT CCA GTA GAT ACA GAG G); *Ccr2* forward and reverse (ACG ATG ATG GTG AGC CTT GTC and CAG GAA GAG CAG GTC AGA GAT G); *IAP* forwards and reverse (ACT AAC TCC TGC TGA CTG G and TGT GGC TTG CTC ATA GAT TAG); *Dnmt1ex3-4* forward and reverse (GAG GAA GGC TAC CTG GCT AAA G and TCA CTG TCC GAC TTG CTT CTC); *MLV* forward and reverse (CCA GAC TTG ATC CTG CTA CA and CTC AGT CAG CCA TCT CTG AC); *LV30* forward and reverse (CTC GCA CCT TTT CGC GCT CG and GCG AGG GGA TCA TCA TAA CA); *Ccl5* forward and reverse (ATA TGG CTC GGA CAC CAC TC and CCC ACT TCT TCT CTG GGT TG); *Mavs* forward and reverse (GGA CAC ACT CTG GGG ACT CT and GGT CAG GGA TGT TGT GAC CT); *Ifit1* forward and reverse (GCT CTG CTG AAA ACC CAG AG and CCC AAT GGG TTC TTG ATG TC); *Ccl5* forward and reverse (CCC TCA CCA TCA TCC TCA CT and GAG CAC TTG CTG CTG GTG TA); *Aim2* forward and reverse (CCT GAT TCA AAG TGC AGG TG and GAG GCA GCA GAG CAG TTT TC); *Il1b* forward and reverse (ACT CAT TGT GGC TGT GGA GA and TTG TTC ATC TCG GAG CCT GT); *Il6* forward and reverse (GAG GAT ACC ACT CCC AAC AGA CC and AAG TGC ATC ATC GTT GTT CAT ACA); *Ifna* forward and reverse (CGC AGG AGA AGG TGG ATG and TGC TGG TGG AGG TCA TTG); *Ifng* forward and reverse (GCT GAC CTA GAG AAG ACA CAT C and TTC CAC ATC TAT GCC ACT TGA G).

qPCR primer for mRNA expression of human genes

B2M forward and reverse (GAG TAT GCC TGC CGT GTG AAC and TCT AAG TTG CCA GCC CTC CTA G); *CCL5* forward and reverse (CTG CTT TGC CTA CAT TGC CC and TCG GGT GAC AAA GAC

GAC TG); *IFT2* forward and reverse (CAA AGG GCA AAA CGA GGC AG and CCC AGG CAT AGT TTC CCC AG).

RNA sequencing and data analysis

For RNA sequencing, epidermis of three control and three *Dnmt1^{Δ/Δep}* mice was isolated at P3 and keratinocytes were cultured as described above for 5 days. RNA was extracted as described above and then used for RNA sequencing. For transcriptome sequencing (RNA-seq) experiments, RNA was subjected to poly(A) selection with a Dynabeads mRNA purification kit (Invitrogen), followed by reverse transcription using a NEB RNA Ultra kit and library generation using a TruSeq library generation kit (Illumina). We performed full-length mRNA-seq experiments in three biological replicates for *Dnmt1^{Δ/Δep}* and the corresponding control keratinocytes and applied the "union" model of the htseq-count script (Anders et al, 2015) to calculate the number of reads associated with each of the 21,608 mouse RefSeq genes for each sample. We used these counts to compute reads per kilobase per million (RPKM) values for each gene and determined Spearman's correlation coefficient (*p*) for each set of biological replicates. Based on the high correlation of the replicates (*P* = 0.99 between each 2 of the 3 control samples and between each 2 of the 3 knockout samples), we used the log-transformed means of RPKM values under each condition to plot the distribution of gene expression levels by using kernel density estimation. Based on this distribution, we set the threshold for gene expression to 1 RPKM (log-RPKM value equal to zero). This is consistent with data from previous studies, which estimated that the value of 1 RPKM corresponds to 1 transcript per cell (Mortazavi et al, 2008). The analysis of differentially expressed genes across the two conditions was performed by using htseq-count and the Bioconductor edgeR package (Gentleman et al, 2004; Robinson et al, 2010). Genes that showed a minimum of a 2-fold change in expression levels (adjusted *P*-value of ≤ 0.05) were classified as upregulated, whereas genes displaying a fold change of ≤ 0.5 (adjusted *P*-value of ≤ 0.05) were categorized as downregulated. The cutoffs for differential expression were set as absolute fold change > 2 , and a corrected *P*-value of > 0.05 . GO analysis was performed with the DAVID (<https://david.ncifcrf.gov/>). The Entrez-GeneIDs of the genes of interest were used as input for the web-based analysis tools. The genes were functionally classified according to the Gene Ontology Consortium annotation category GO biological process.

Repeat analysis

To analyze repeat enrichment, we mapped the reads with bowtie (Langmead et al, 2009) (v 1.2.0, -m1 --max multi.fastq) against the human reference genome (GRCh38) or the mouse reference genome (MGSCv37). The uniquely aligning reads and the multi-mappers were assigned to repeat classes, families, and types with RepEnrich (Criscione et al, 2014). The significantly differentially detected repeats were called using DESeq2 (Love et al, 2014) (v 1.10.1). The repeat count table from repseq was annotated with the class/family name of the repeat and plotted in a scatter plot of log fold change versus log₁₀(adjusted *P*-values).

RNA-seq analysis

The 3' adaptors were removed using cutadapt (v1.4.2, Read1: cutadapt --match-read-wildcards -O 1 -a AGA TCG GAA GAG CAC ACG

TCT GAA CTC CAG TCA C), and trimmed reads with a length of less than 18 bp were discarded. The trimmed reads were filtered with a contaminants database consisting of rDNA sequences (KY962518.1, NR_023363.1 and the ERCC.fa) with bowtie2 (v2.1.0 --very-sensitive-local). The recovered nonmatching reads were aligned to the genome/transcriptome using STAR-align (v2.4.2a, STAR --outSAMstrandField None --outFilterIntronMotifs RemoveNoncanonical --outFilterMismatchNoverLmax 0.1 --outFilterMismatchNmax 10 --outFilterScoreMinOverLread 0.30 --outFilterMatchNminOverLread 0.30 --outFilterMatchNmin 30 --chimSegmentMin 15 --quantMode TranscriptomeSAM --chimJunctionOverhangMin 15 --twopassMode Basic --outSAMtype SAM --outSAMattributes All --outReadsUnmapped Fastx intronMotif --alignIntronMax 200000 --outSJfilterIntronMaxVsReadN 10000 20000 30000 50000 --outSJfilterOverhangMin 20 12 12 12 --outFilterType BySJout --alignMatesGapMax 0 --outFilterMultimapNmax 20). The STAR-index used for alignment was generated from the human genome build NCBI GRCh38 (GCA_000001405.15) and a transcriptome GTF file from ENSEMBL build 78. Unique mappers from the resulting BAM file were used to create unstranded, stranded and reverse stranded coverage tracks for visualization using bedtools (v2.27, bedtools genomecov -split -bg, bedtools genomecov -split -bg -strand "+", bedtools genomecov -split -bg -strand "-") and bedGraphToBigWig from the kent-tools (bedGraphToBigWig v4, bedGraphToBigWig -blockSize=256 -itemsPerSlot=1024). Normalized coverage tracks were created by dividing the coverage at each position with the total number of aligned reads per million. The differentially expressed genes were called using DESeq2 (Love et al, 2014) (v 1.10.1).

Protein and histone isolation and immunoblot analysis

Protein and isolation from skin and cultured keratinocytes for immunoblot analysis and subsequent immunoblot signal quantification were performed as previously described (Winter et al, 2013).

Primary antibodies for immunoblotting

DNMT1 (1:500, sc-20701, Santa Cruz Biotechnology), DNMT3a (1:1,000, sc-20703, Santa Cruz Biotechnology), DNMT3b (1:1,000, sc-376043, Santa Cruz Biotechnology), Actin (1:20,000; A5316, Sigma), Lamin B (1:1,000, sc-6216, Santa Cruz Biotechnology), H3 C-terminal (1:500,000, ab1791, Abcam), IAP (1:500, kindly provided by the Bryan R. Cullen lab (Bogerd et al, 2006), Center for Virology and Department of Molecular Genetics and Microbiology, Duke University Medical Center, Durham), PCNA (1:1,000, C1 PC10, Dako), γ H2A.X S139ph (1:1,000, ab2893, Abcam), and cGas (1:1,000, 31659, Cell Signaling).

FACS analysis

Dermis and epidermis from pups were separated after overnight incubation in dispase solution (see above) at 4°C. Epidermis was cut into small pieces and incubated for 30 min at 37°C in 0.2 mg/ml DNase I (Sigma) in RPMI. Dermis was cut and treated with RPMI containing DNase and 1.6 mg/ml collagenase IV (Worthington) for 30 min at 37°C. A single cell suspension was prepared by passing the dissociated tissue through a 70- μ m cell strainer. Cells were washed with FACS buffer (1% BSA, 0.1% NaN₃, PBS), and unspecific antibody binding was blocked with anti-mouse CD16/CD32 (eBioscience). Approximately 1×10^6 cells per tube were stained

with respective antibodies for 30 min at 4°C. 7AAD (Sigma) was added shortly before measurement for dead cell discrimination. Data were acquired on an FACS-Aria and analyzed with FlowJo software according to the gating strategy shown in Appendix Fig S10.

Primary antibodies used for FACS

CD45 APC-Cy7 (1:100, BioLegend, clone 30-F11), MHC-II PE (1:1,000, BioLegend, clone M5), CD11b PE-Cy7 (1:100, BioLegend, clone M1/70), F4/80 APC (1:50, eBioscience, clone BM8), Ly6G PE (1:50, BioLegend), and 7AAD PerCP (2.5 μ l/sample, Sigma).

Quantifications and Statistical analysis

Quantification of Ki67 and Histone H3S10ph (H3S10ph) epidermal cells

Paraffin sections of back skin from P7 wild-type and *Dnmt1* ^{Δ/Δ ep} mice were double immunolabeled for Ki67 and H3S10ph. For quantification, three random images per mouse were chosen and the number of basal and suprabasal epidermal H3S10ph-positive and Ki67/H3S10ph double-positive nuclei were counted in a blinded manner. The obtained triplicate values were averaged and compared with an unpaired two-tailed *t*-test.

Statistical analysis

In general, measurements were taken from distinct samples. qRT-PCR and quantification experiments were evaluated with Microsoft Excel. Immunoblot signal intensities were quantified using the ImageQuants software, and relative protein levels were normalized to beta-Actin or Lamin B. The significance between groups was determined by the unpaired Student's *t*-test or by ANOVA. *P*-values were calculated with the GraphPad Prism software, and standard deviation (s.d.) or standard error of the mean (SEM) is shown. **P* \leq 0.05; ***P* \leq 0.01; ****P* \leq 0.001; ns = not significant (*P* > 0.05).

Quantification of micronuclei

PicoGreen-stained cells were scanned using a 100x oil immersion objective. The scans were randomized, and 6 images each were blindly selected for analysis. Micronucleus-associated nuclei were counted along with the total number of nuclei.

Data availability

The RNA-seq datasets have been deposited to the NCBI Gene Expression Omnibus (GEO) under GSE166356 (<http://www.ncbi.nlm.nih.gov/geo/query/acc.cgi?acc=GSE166356>).

Expanded View for this article is available online.

Acknowledgements

This work was supported by the Austrian Science Fund (P28705, P28034, P34998, SFB F70), GEN-AU project "Epigenetic Regulation of Cell Fate Decisions" (Federal Ministry for Education, Science, and Culture) and the University of Vienna Initiativkolleg I031-B to CS. MAB was a fellow of the International PhD program "Molecular Mechanisms of Cell Signaling" supported by the Austrian Science Fund (W1220). We thank Christopher B Wilson for providing the *Dnmt1* *fl/fl* mice (Lee et al., 2001), Ulrich Elling for the DNMT1 KO ES cells, and Bryan R. Cullen for the IAP antibody. We thank Leopold Eckhart, Beate

Lichtenberger, Astrid Hagelkruys, Adrian Bird, Josipa Raguz, Luisa Seufert, Manuela Baccarini, Thomas Decker, Nicole Amberg, and Sabbi Lall for fruitful discussions. We like to thank Brigitte Gundacker, Jelena Marjanovic, Alexandra Stiegler, Irmgard Fischer, and Petra Kodajova for technical support, and Maggie Goiser for bioinformatic support. We are grateful to the teams of the MPL animal facility and the animal facility at the CACB (Robert Vilvoi) and the Vienna Biocenter NGS facility for their continuous support.

Author contributions

CSe, MAB, HF, and MW conceptualized the study. CSe, MAB, HF, MW, MS, and AA designed the study. MAB, HF, MW, LG, SS, PW, TG, TM, BZ, CFi, Cfo, JA, BR, SL, GM, AP, MK, GE, MM, and CSch carried out experiments. ST, UR, MG, PP, and LK analyzed data. IT and RST carried out bioinformatic analysis. CSe, MAB and HF wrote the manuscript.

Conflict of interest

The authors declare that they have no conflict of interest.

References

- Ablasser A, Hur S (2020) Regulation of cGAS- and RLR-mediated immunity to nucleic acids. *Nat Immunol* 21: 17–29
- Ahn J, Gutman D, Saijo S, Barber GN (2012) STING manifests self DNA-dependent inflammatory disease. *Proc Natl Acad Sci USA* 109: 19386–19391
- Alonso L, Fuchs E (2003) Stem cells of the skin epithelium. *Proc Natl Acad Sci USA* 100(Suppl 1): 11830–11835
- Alvarez-Errico D, Vento-Tormo R, Ballestar E (2017) Genetic and epigenetic determinants in autoinflammatory diseases. *Front Immunol* 8: 318
- Anders S, Pyl PT, Huber W (2015) HTSeq—a Python framework to work with high-throughput sequencing data. *Bioinformatics* 31: 166–169
- Ambrosi C, Manzo M, Baubec T (2017) Dynamics and context-dependent roles of DNA methylation. *J Mol Biol* 429: 1459–1475
- Arand J, Spieler D, Karius T, Branco MR, Meilinger D, Meissner A, Jenuwein T, Xu G, Leonhardt H, Wolf V et al (2012) In vivo control of CpG and non-CpG DNA methylation by DNA methyltransferases. *PLoS Genet* 8: e1002750
- Bakhomou SF, Ngo B, Laughney AM, Cavallo J-A, Murphy CJ, Ly P, Shah P, Sriram RK, Watkins TBK, Taunk NK et al (2018) Chromosomal instability drives metastasis through a cytosolic DNA response. *Nature* 553: 467–472
- Bartok E, Hartmann G (2020) Immune Sensing Mechanisms that Discriminate Self from Altered Self and Foreign Nucleic Acids. *Immunity* 53: 54–77
- Boger DP, Wiegand HL, Doehle BP, Lueders KK, Cullen BR (2006) APOBEC3A and APOBEC3B are potent inhibitors of LTR-retrotransposon function in human cells. *Nucleic Acids Res* 34: 89–95
- Briso EM, Guinea-Viniegra J, Bakiri L, Rogon Z, Petzelbauer P, Eils R, Wolf R, Rincon M, Angel P, Wagner EF (2013) Inflammation-mediated skin tumorigenesis induced by epidermal c-Fos. *Genes Dev* 27: 1959–1973
- Chatterjee R, He X, Huang D, FitzGerald P, Smith A, Vinson C (2014) High-resolution genome-wide DNA methylation maps of mouse primary female dermal fibroblasts and keratinocytes. *Epigenetics Chromatin* 7: 35
- Chen T, Hevi S, Gay F, Tsujimoto N, He T, Zhang B, Ueda Y, Li E (2007) Complete inactivation of DNMT1 leads to mitotic catastrophe in human cancer cells. *Nat Genet* 39: 391–396
- Chiappinelli K, Strissel P, Desrichard A, Li H, Henke C, Akman B, Hein A, Rote N, Cope L, Snyder A et al (2015) Inhibiting DNA methylation causes an interferon response in cancer via dsRNA including endogenous retroviruses. *Cell* 162: 974–986
- Costa G, Barra V, Lentini L, Cilluffo D, Di Leonardo A (2016) DNA demethylation caused by 5-Aza-2'-deoxycytidine induces mitotic alterations and aneuploidy. *Oncotarget* 7: 3726–3739
- Criscione SW, Zhang Y, Thompson W, Sedivy JM, Neretti N (2014) Transcriptional landscape of repetitive elements in normal and cancer human cells. *BMC Genom* 15: 583
- Daver N, Boddu P, Garcia-Manero G, Yadav SS, Sharma P, Allison J, Kantarjian H (2018) Hypomethylating agents in combination with immune checkpoint inhibitors in acute myeloid leukemia and myelodysplastic syndromes. *Leukemia* 32: 1094–1105
- Devos M, Tanghe G, Gilbert B, Dierick E, Verheirstraeten M, Nemegeer J, de Reuver R, Lefebvre S, De Munck J, Rehwinkel J et al (2020) Sensing of endogenous nucleic acids by ZBP1 induces keratinocyte necroptosis and skin inflammation. *J Exp Med* 217: e20191913
- Dou Z, Ghosh K, Vizioli MG, Zhu J, Sen P, Wangenstein KJ, Simithy J, Lan Y, Lin Y, Zhou Z et al (2017) Cytoplasmic chromatin triggers inflammation in senescence and cancer. *Nature* 550: 402–406
- Elliott EN, Sheaffer KL, Schug J, Stappenbeck TS, Kaestner KH (2015) Dnmt1 is essential to maintain progenitors in the perinatal intestinal epithelium. *Development* 142: 2163–2172
- Espada J, Esteller M (2010) DNA methylation and the functional organization of the nuclear compartment. *Semin Cell Dev Biol* 21: 238–246
- Fan G, Beard C, Chen RZ, Csankovszki G, Sun YI, Siniatia M, Biniszkiwicz D, Bates B, Lee PP, Kühn R et al (2001) DNA hypomethylation perturbs the function and survival of CNS neurons in postnatal animals. *J Neurosci* 21: 788–797
- Fenech M, Kirsch-Volders M, Natarajan AT, Surrallés J, Crott JW, Parry J, Norppa H, Eastmond DA, Tucker JD, Thomas P (2011) Molecular mechanisms of micronucleus, nucleoplasmic bridge and nuclear bud formation in mammalian and human cells. *Mutagenesis* 26: 125–132
- Fischer H, Rossiter H, Ghannadan M, Jaeger K, Barresi C, Declercq W, Tschachler E, Eckhart L (2005) Caspase-14 but not caspase-3 is processed during the development of fetal mouse epidermis. *Differentiation* 73: 406–413
- Flood BA, Higgs EF, Li S, Luke JJ, Gajewski TF (2019) STING pathway agonism as a cancer therapeutic. *Immunol Rev* 290: 24–38
- Fuchs E, Horsley V (2008) More than one way to skin. *Genes Dev* 22: 976–985
- Gao D, Li T, Li XD, Chen X, Li QZ, Wight-Carter M, Chen ZJ (2015) Activation of cyclic GMP-AMP synthase by self-DNA causes autoimmune diseases. *Proc Natl Acad Sci USA* 112: E5699–E5705
- Gaudet F, Rideout 3rd WM, Meissner A, Dausman J, Leonhardt H, Jaenisch R (2004) Dnmt1 expression in pre- and postimplantation embryogenesis and the maintenance of IAP silencing. *Mol Cell Biol* 24: 1640–1648
- Gentleman RC, Carey VJ, Bates DM, Bolstad B, Dettling M, Dudoit S, Ellis B, Gautier L, Ge Y, Gentry J et al (2004) Bioconductor: open software development for computational biology and bioinformatics. *Genome Biol* 5: R80
- Georgia S, Kanji M, Bhushan A (2013) DNMT1 represses p53 to maintain progenitor cell survival during pancreatic organogenesis. *Genes Dev* 27: 372–377
- Gluck S, Guey B, Gulen MF, Wolter K, Kang TW, Schmacke NA, Bridgeman A, Rehwinkel J, Zender L, Ablasser A (2017) Innate immune sensing of cytosolic chromatin fragments through cGAS promotes senescence. *Nat Cell Biol* 19: 1061–1070
- Gray EE, Treuting PM, Woodward JJ, Stetson DB (2015) Cutting edge: cGAS is required for lethal autoimmune disease in the Trex1-deficient mouse model of Aicardi-Goutieres Syndrome. *J Immunol* 195: 1939–1943

- Gudjonsson JE, Krueger G (2012) A role for epigenetics in psoriasis: methylated Cytosine-Guanine sites differentiate lesional from nonlesional skin and from normal skin. *J Invest Dermatol* 132: 506–508
- Haag SM, Gulen MF, Reymond L, Gibelin A, Abrami L, Decout A, Heymann M, van der Goot FG, Turcatti G, Behrendt R et al (2018) Targeting STING with covalent small-molecule inhibitors. *Nature* 559: 269–273
- Han J, Park SG, Bae JB, Choi J, Lyu JM, Park SH, Kim HS, Kim YJ, Kim S, Kim TY (2012) The characteristics of genome-wide DNA methylation in naive CD4+ T cells of patients with psoriasis or atopic dermatitis. *Biochem Biophys Res Comm* 422: 157–163
- Hogg SJ, Beavis PA, Dawson MA, Johnstone RW (2020) Targeting the epigenetic regulation of antitumour immunity. *Nature Reviews Drug Discov* 19: 776–800
- Hoong BYD, Gan YH, Liu H, Chen ES (2020) cGAS-STING pathway in oncogenesis and cancer therapeutics. *Oncotarget* 11: 2930–2955
- Jackson-Grusby L, Beard C, Possemato R, Tudor M, Fambrough D, Csankovszki G, Dausman J, Lee P, Wilson C, Lander E et al (2001) Loss of genomic methylation causes p53-dependent apoptosis and epigenetic deregulation. *Nat Genet* 27: 31–39
- Javierre BM, Hernando H, Ballestar E (2012) Environmental triggers and epigenetic deregulation in autoimmune disease. *Discov Med* 12: 535–545
- Jiao H, Wachsmuth L, Kumari S, Schwarzer R, Lin J, Eren RO, Fisher A, Lane R, Young GR, Kassiotis G et al (2020) Z-nucleic-acid sensing triggers ZBP1-dependent necroptosis and inflammation. *Nature* 580: 391–395
- Jones PA, Issa JP, Baylin S (2016) Targeting the cancer epigenome for therapy. *Nat Rev Genet* 17: 630–641
- Jones PA, Ohtani H, Chakravarthy A, De Carvalho DD (2019) Epigenetic therapy in immune-oncology. *Nat Rev Cancer* 19: 151–161
- Kabashima K, Honda T, Ginhoux F, Egawa G (2019) The immunological anatomy of the skin. *Nat Rev Immunol* 19: 19–30
- Karemaker ID, Baubec T (2020) DNA methyltransferases hitchhiking on chromatin. *Swiss Med Wkly* 150: w20329
- Kawai T, Akira S (2011) Toll-like receptors and their crosstalk with other innate receptors in infection and immunity. *Immunity* 34: 637–650
- de Koning HD, Bergboer JG, van den Bogaard EH, van Vlijmen-Willems IM, Rodijk-Olthuis D, Simon A, Zeeuwen PL, Schalkwijk J (2012) Strong induction of AIM2 expression in human epidermis in acute and chronic inflammatory skin conditions. *Exp Dermatol* 21: 961–964
- Kwon J, Bakhomou SF (2020) The Cytosolic DNA-Sensing cGAS-STING Pathway in Cancer. *Cancer Discov* 10: 26–39
- Lai J, Fu Y, Tian S, Huang S, Luo X, Lin L, Zhang X, Wang H, Lin Z, Zhao H et al (2021) Zebularine elevates STING expression and enhances cGAMP cancer immunotherapy in mice. *Mol Ther* 29: 1758–1771
- Langmead B, Trapnell C, Pop M, Salzberg SL (2009) Ultrafast and memory-efficient alignment of short DNA sequences to the human genome. *Genome Biol* 10: R25
- Lee PP, Fitzpatrick DR, Beard C, Jessup HK, Lehar S, Makar KW, Pérez-Melgosa M, Sweetser MT, Schissel MS, Nguyen S et al (2001) A critical role for Dnmt1 and DNA methylation in T cell development, function, and survival. *Immunity* 15: 763–774
- Leyvraz C, Charles RP, Rubera I, Guitard M, Rotman S, Breiden B, Sandhoff K, Hummler E (2005) The epidermal barrier function is dependent on the serine protease CAP1/Prss8. *J Cell Biol* 170: 487–496
- Li E, Bestor TH, Jaenisch R (1992) Targeted mutation of the DNA methyltransferase gene results in embryonic lethality. *Cell* 69: 915–926
- Li J, Jiang TX, Hughes MW, Wu P, Yu J, WidELITZ RB, Fan G, Chuong CM (2012) Progressive alopecia reveals decreasing stem cell activation probability during aging of mice with epidermal deletion of DNA methyltransferase 1. *J Invest Dermatol* 132: 2681–2690
- Li X, Zhang Q, Ding Y, Liu Y, Zhao D, Zhao K, Shen Q, Liu X, Zhu X, Li N et al (2016) Methyltransferase Dnmt3a upregulates HDAC9 to deacetylate the kinase TBK1 for activation of antiviral innate immunity. *Nat Immunol* 17: 806–815
- Licht JD (2015) DNA methylation inhibitors in cancer therapy: the immunity dimension. *Cell* 162: 938–939
- Love MI, Huber W, Anders S (2014) Moderated estimation of fold change and dispersion for RNA-seq data with DESeq2. *Genome Biol* 15: 550
- Lutsik P, Feuerbach L, Arand J, Lengauer T, Walter J, Bock C (2011) BiQ Analyzer HT: locus-specific analysis of DNA methylation by high-throughput bisulfite sequencing. *Nucleic Acids Res* 39: W551–W556
- Ma F, Li B, Liu SY, Iyer SS, Yu Y, Wu A, Cheng G (2015) Positive feedback regulation of type I IFN production by the IFN-inducible DNA sensor cGAS. *J Immunol* 194: 1545–1554
- Mackenzie KJ, Carroll P, Martin C-A, Murina O, Fluteau A, Simpson DJ, Olova N, Sutcliffe H, Rainger JK, Leitch A et al (2017) cGAS surveillance of micronuclei links genome instability to innate immunity. *Nature* 548: 461–465
- Magoc T, Salzberg SL (2011) FLASH: fast length adjustment of short reads to improve genome assemblies. *Bioinformatics* 27: 2957–2963
- Mannion N, Greenwood SM, Young R, Cox S, Brindle J, Read D, Nellåker C, Vesely C, Ponting C, McLaughlin P et al (2014) The RNA-editing enzyme ADAR1 controls innate immune responses to RNA. *Cell Rep* 9: 1482–1494
- Martin M (2011) Cutadapt removes adapter sequences from high-throughput sequencing reads. *EMBnetjournal* 17: 10
- McLaughlin LJ, Stojanovic L, Kogan AA, Rutherford JL, Choi EY, Yen R-W, Xia L, Zou Y, Lapidus RG, Baylin SB et al (2020) Pharmacologic induction of innate immune signaling directly drives homologous recombination deficiency. *Proc Natl Acad Sci USA* 117: 17785–17795
- Mehdipour P, Marhon SA, Ettayebi I, Chakravarthy A, Hosseini A, Wang Y, de Castro FA, Loo Yau H, Ishak C, Abelson S et al (2020) Epigenetic therapy induces transcription of inverted SINES and ADAR1 dependency. *Nature* 588: 169–173
- Melki I, Fremont ML (2020) Type I Interferonopathies: from a Novel Concept to Targeted Therapeutics. *Curr Rheumatol Rep* 22: 32
- Mikkola ML (2007) Genetic basis of skin appendage development. *Semin Cell Dev Biol* 18: 225–236
- Miroshnikova YA, Cohen I, Ezhkova E, Wickstrom SA (2019) Epigenetic gene regulation, chromatin structure, and force-induced chromatin remodeling in epidermal development and homeostasis. *Curr Opin Genet Dev* 55: 46–51
- Mohan KN, Chaillet JR (2013) Cell and molecular biology of DNA methyltransferase 1. *Int Rev Cell Mol Biol* 306: 1–42
- Morita M, Stamp G, Robins P, Dulic A, Rosewell I, Hrivnak G, Daly G, Lindahl T, Barnes DE (2004) Gene-targeted mice lacking the Trex1 (DNase III) 3'–>5' DNA exonuclease develop inflammatory myocarditis. *Mol Cell Biol* 24: 6719–6727
- Mortazavi A, Williams BA, McCue K, Schaeffer L, Wold B (2008) Mapping and quantifying mammalian transcriptomes by RNA-Seq. *Nat Methods* 5: 621–628
- Nguyen AV, Soulika AM (2019) The dynamics of the Skin's immune system. *Int J Mol Sci* 20: 1811
- Ramirez A, Page A, Gandarillas A, Zanet J, Pibre S, Vidal M, Tusell L, Genesca A, Whitaker DA, Melton DW et al (2004) A keratin K5Cre transgenic line appropriate for tissue-specific or generalized Cre-mediated recombination. *Genesis* 39: 52–57

- Ramsahoye BH (2002) Measurement of genome-wide DNA cytosine-5 methylation by reversed-phase high-pressure liquid chromatography. *Methods Mol Biol* 200: 17–27
- Rigby RE, Webb LM, Mackenzie KJ, Li Y, Leitch A, Reijns MAM, Lundie RJ, Revuelta A, Davidson DJ, Diebold S *et al* (2014) RNA:DNA hybrids are a novel molecular pattern sensed by TLR9. *EMBO J* 33: 542–558
- Robinson MD, McCarthy DJ, Smyth GK (2010) edgeR: a Bioconductor package for differential expression analysis of digital gene expression data. *Bioinformatics* 26: 139–140
- Rodríguez E, Baurecht H, Wahn AF, Kretschmer A, Hotze M, Zeilinger S, Klopp N, Illig T, Schramm K, Prokisch H *et al* (2014) An integrated epigenetic and transcriptomic analysis reveals distinct tissue-specific patterns of DNA methylation associated with atopic dermatitis. *J Invest Dermatol* 134: 1873–1883
- Roers A, Hiller B, Hornung V (2016) Recognition of endogenous nucleic acids by the innate immune system. *Immunity* 44: 739–754
- Roulois D, Loo Yau H, Singhania R, Wang Y, Danesh A, Shen S, Han H, Liang G, Jones P, Pugh T *et al* (2015) DNA-demethylating agents target colorectal cancer cells by inducing viral mimicry by endogenous transcripts. *Cell* 162: 961–973
- Schindelin J, Arganda-Carreras I, Frise E, Kaynig V, Longair M, Pietzsch T, Preibisch S, Rueden C, Saalfeld S, Schmid B *et al* (2012) Fiji: an open-source platform for biological-image analysis. *Nat Methods* 9: 676–682
- Schlee M, Hartmann G (2016) Discriminating self from non-self in nucleic acid sensing. *Nat Rev Immunol* 16: 566–580
- Shoggins JW, MacDuff DA, Imanaka N, Gainey MD, Shrestha B, Eitson JL, Mar KB, Richardson RB, Ratushny AV, Litvak V *et al* (2014) Pan-viral specificity of IFN-induced genes reveals new roles for cGAS in innate immunity. *Nature* 505: 691–695
- Schubeler D (2015) Function and information content of DNA methylation. *Nature* 517: 321–326
- Sen GL, Reuter JA, Webster DE, Zhu L, Khavari PA (2010) DNMT1 maintains progenitor function in self-renewing somatic tissue. *Nature* 463: 563–567
- Sheaffer KL, Kim R, Aoki R, Elliott EN, Schug J, Burger L, Schubeler D, Kaestner KH (2014) DNA methylation is required for the control of stem cell differentiation in the small intestine. *Genes Dev* 28: 652–664
- Sibilia M, Fleischmann A, Behrens A, Stingl L, Carroll J, Watt FM, Schlessinger J, Wagner EF (2000) The EGF receptor provides an essential survival signal for SOS-dependent skin tumor development. *Cell* 102: 211–220
- Simon M, Van Meter M, Ablaeva J, Ke Z, Gonzalez RS, Taguchi T, De Cecco M, Leonova KI, Kogan V, Helfand SL *et al* (2019) LINE1 derepression in aged wild-type and SIRT6-deficient mice drives inflammation. *Cell Metab* 29: 871–885.e5
- Smith ZD, Meissner A (2013) DNA methylation: roles in mammalian development. *Nat Rev Genet* 14: 204–220
- Stopper H, Korber C, Schiffmann D, Caspary WJ (1993) Cell-cycle dependent micronucleus formation and mitotic disturbances induced by 5-azacytidine in mammalian cells. *Mutat Res* 300: 165–177
- Stresemann C, Lyko F (2008) Modes of action of the DNA methyltransferase inhibitors azacytidine and decitabine. *Int J Cancer* 123: 8–13
- Sun Q, Sun L, Liu HH, Chen X, Seth RB, Forman J, Chen ZJ (2006) The specific and essential role of MAVS in antiviral innate immune responses. *Immunity* 24: 633–642
- Swanson KV, Junkins RD, Kurkjian CJ, Holley-Guthrie E, Pendse AA, El Morabiti R, Petrucelli A, Barber GN, Benedict CA, Ting JP (2017) A noncanonical function of cGAMP in inflammasome priming and activation. *J Exp Med* 214: 3611–3626
- Tsumura A, Hayakawa T, Kumaki Y, Takebayashi S-I, Sakaue M, Matsuoka C, Shimotohno K, Ishikawa F, Li EN, Ueda HR *et al* (2006) Maintenance of self-renewal ability of mouse embryonic stem cells in the absence of DNA methyltransferases Dnmt1, Dnmt3a and Dnmt3b. *Genes Cells* 11: 805–814
- Uggetti C, Lepelley A, Crow YJ (2019) Self-awareness: nucleic acid-driven inflammation and the type I interferonopathies. *Annu Rev Immunol* 37: 247–267
- Wagner T, Gschwandtner M, Strajeriu A, Elbe-Burger A, Grillari J, Grillari-Voglauer R, Greiner G, Golabi B, Tschachler E, Mildner M (2018) Establishment of keratinocyte cell lines from human hair follicles. *Sci Rep* 8: 13434
- Winter M, Moser MA, Meunier D, Fischer C, Machat G, Mattes K, Lichtenberger BM, Brunmeir R, Weissmann S, Murko C *et al* (2013) Divergent roles of HDAC1 and HDAC2 in the regulation of epidermal development and tumorigenesis. *EMBO J* 32: 3176–3191
- Xu GL, Bestor TH, Bourc'his D, Hsieh CL, Tommerup N, Bugge M, Hulten M, Qu X, Russo JJ, Viegas-Pequignot E (1999) Chromosome instability and immunodeficiency syndrome caused by mutations in a DNA methyltransferase gene. *Nature* 402: 187–191
- Yum S, Li M, Chen ZJ (2020) Old dogs, new trick: classic cancer therapies activate cGAS. *Cell Res* 30: 639–648
- Zheng Y, Danilenko DM, Valdez P, Kasman I, Eastham-Anderson J, Wu J, Ouyang W (2007) Interleukin-22, a T(H)17 cytokine, mediates IL-23-induced dermal inflammation and acanthosis. *Nature* 445: 648–651
- Zupkovitz G, Kabiljo J, Kothmayer M, Schlick K, Schofer C, Lagger S, Pusch O (2021) Analysis of methylation dynamics reveals a tissue-specific, age-dependent decline in 5-methylcytosine within the genome of the vertebrate aging model *Nothobranchius furzeri*. *Front Mol Biosci* 8: 627143



License: This is an open access article under the terms of the Creative Commons Attribution License, which permits use, distribution and reproduction in any medium, provided the original work is properly cited.